Supplement of Biogeosciences, 22, 2023–2047, 2025
https://doi.org/10.5194/bg-22-2023-2025-supplement

Biogeosciences
Open Access

Supplement of

Evaluation of long-term carbon dynamics in a drained forested peatland using the ForSAFE-Peat model

Daniel Escobar et al.

Correspondence to: Daniel Escobar (daniel.escobar@natgeo.su.se)

Supplementary material.

1 Detailed model explanation.

A general description of the previous version of the ForSAFE model can be found in Wallman et al. (2005). The model simulates plant dynamics based on the PnET-CN model (Aber et al., 1997), soil chemistry based on the SAFE model (Alveteg et al., 1998; Warfvinge et al., 1993), water dynamics based on the HBV/PULSE model (Andersson, 1988; Bergström, 1991) and soil decomposition dynamics based on the DECOMP model (Wallman et al., 2006; Walse et al., 1998). The model was further developed to include daily dynamics among other processes, such as lateral water movement, by Yu et al. (2018) and Zanchi et al. (2021).

In this contribution, we refined the plant's carbon allocation and respiratory processes. Given different turnover and growing rates between foliage and roots, allocation to roots is constantly recalculated to follow foliage demand. Maintenance respiration is decoupled from photosynthesis and is now a function of plant tissue biomass and temperature. To better capture soil dynamics in peats, this version introduces a dynamic soil volume approach and considers the anaerobic decomposition of soil organic matter. Furthermore, soil nitrogen mineralisation and mineral nitrogen transformations have been changed to recreate better soil microbial processes. Soil organic matter decomposition is coupled with a fixed microbial carbon to nitrogen ratio to calculate mineralisation and immobilisation. In contrast, mineral nitrogen is transformed through nitrification and denitrification with explicitly modelled microbial groups. The description of soil temperature dynamics has been improved by solving the heat equation tailored for peat soils.

While this description primarily focuses on carbon dynamics, other subcomponents are briefly explained, emphasising changes made in this contribution. Carbon is represented as a set of compartments that denote different states of carbon within the system, such as carbon within foliage biomass, labile carbon allocated to roots, cellulose-like carbon in the soil, and so forth. Figure S1 summarises a schematic of organic carbon compartments within the model.

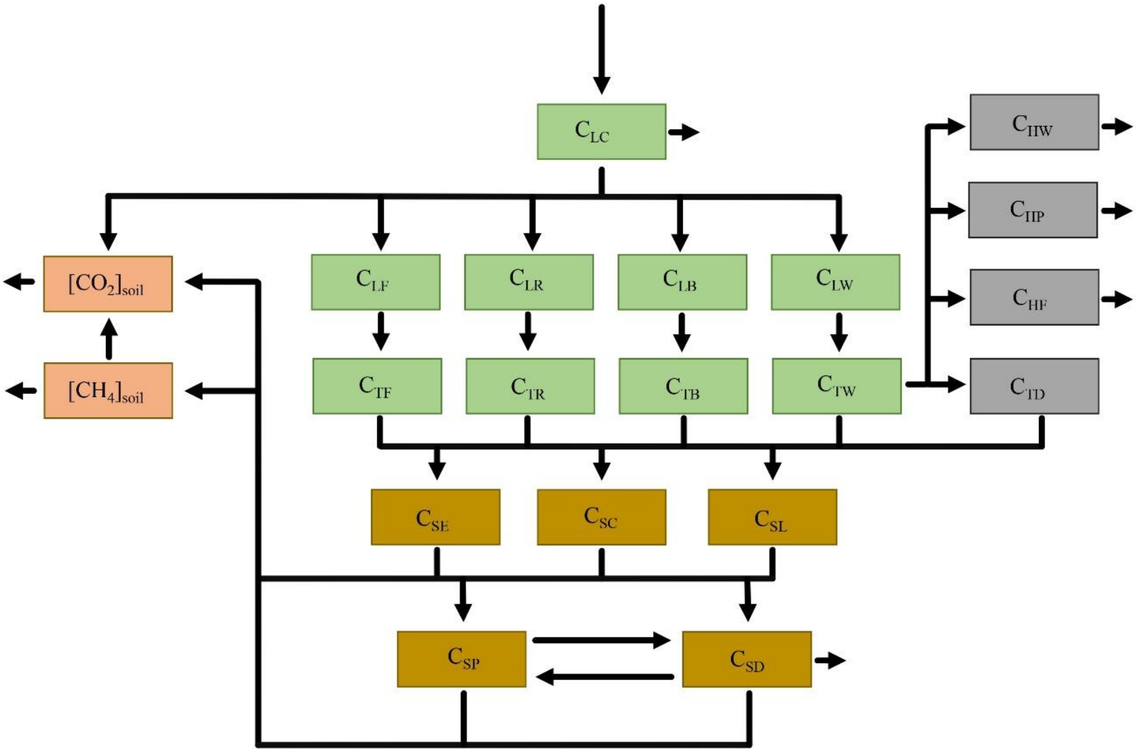

Figure S1. Scheme of carbon compartments within the model. The green boxes represent plant-related compartments, the brown boxes represent soil organic matter compartments, the grey boxes represent deadwood left after harvesting and harvested wood products (HWP), and the pink boxes represent CO2 and CH4 in the soil. The black arrows indicate carbon fluxes, with arrows not connected to any compartment representing fluxes leaving the system. The subscripts denote specific carbon compartments: LC (labile central), LF (labile foliage), LR (labile root), LB (labile branch), LW (labile wood), TF (tissue foliage), TR (tissue root), TB (tissue branch), TW (tissue wood), HW (hardwood from harvest), HP (paper from harvest), HF (fuel from harvesting), TD (tissue deadwood), SE (soil easily decomposable compounds), SC (soil cellulose), SL (soil lignin), SP (soil peat) and SD (soil dissolved).

1.1 Plant carbon dynamics

The PnET model, developed by Aber & Federer (1992), forms the foundation for describing plant carbon dynamics. PnET is a big-leaf model where maximum assimilation per unit of leaf mass is a function of leaf nitrogen concentration and is further influenced by day length, atmospheric CO_2 concentration, and air temperature. At the same time, it is reduced by vapour pressure deficit (VPD). Maximum assimilation is expressed as,

$$Amax = \left(\alpha_{Amax} + \beta_{Amax} * \frac{\mathrm{N_{TF}}}{\mathrm{C_{TF}}} * C_P : DW_P * 100 * MR\right) * \ DL * \ \frac{12}{10^9} * f_{CO_2} * \ f_{Tair} * f_{VPD}. \qquad \textbf{(1)}$$

In equation 1, $Amax$ is the maximum assimilation per unit of leaf dry weight per day (g_C g^{-1} $_{DW}$ d^{-1}), α_{Amax} is the intercept ($nmol_{CO2}$ g^{-1}_{DW} s^{-1}), β_{Amax} is the slope ($nmol_{CO2}$ g_N s^{-1}) of the function linking $Amax$ to foliage nitrogen concertation, $\mathrm{N_{TF}}$ is nitrogen content in foliage tissue (g_N m^{-2}_{soil}), C_{TF} is carbon content in foliage tissue (g_C m^{-2}_{soil}), $C_P\!:DW_P$ is the carbon to dry weight ratio (g_C g^{-1}_{DW}), 100 transforms the ratio of nitrogen content to carbon content into a percentage, MR **(**dimensionless) is the assimilation as a fraction of the morning rate and, DL is the day length (s d^{-1}) calculated based on coordinates and day of the year. The model integrates environmental factors affecting photosynthesis by adjusting Amax using scaling functions based on environmental parameters.

Photosynthesis is modulated by atmospheric CO_2 through the linear function $f_{\mathrm{CO_2}}$,

$$f_{CO_2} \;=\; 1 + \frac{f_{CO_2atm} - f_{CO_2350}}{f_{CO_2350}}, \qquad \textbf{(2)}$$

where,

$$f_{CO_2atm} = \frac{[CO_2]_{atm} * \mathrm{C}F{:}CA - 68}{[CO_2]_{atm} * \mathrm{C}F{:}CA + 136}, \qquad \textbf{(3)}$$

$$f_{CO_2350} = \frac{350 * \mathrm{C}F{:}CA - 68}{350 * \mathrm{C}F{:}CA + 136}. \qquad \textbf{(4)}$$

$[CO_2]_{atm}$ is the daily atmospheric concentration of CO_2 (ppm) while background CO_2 atmospheric concentration is set to 350 CO_2 ppm. $CF\!:CA$ is the ratio between the leaf CO_2 concentration and the atmospheric CO_2 concentration,

$$CL\!:CA \;=\; -0.075 * \frac{\mathrm{N_{TF}}}{\mathrm{C_{TF}}} * C_P\!:DW_P * 100 + 0.875. \qquad \textbf{(5)}$$

Temperature also affects maximum gross photosynthesis through f_{Tair} as follows,

$$f_{Tair} \;=\; \frac{(PTmax - Tave) * (Tave - PTmin)}{\left(\frac{PTmax - PTmin}{2}\right)^2}, \qquad \textbf{(6)}$$

where $PTmax$ (°C) is the maximum air temperature for photosynthesis, $PTmin$ (°C) is the minimum air temperature for photosynthesis, and $Tave$ (°C) is the average air temperature during the time step.
The function f_{VPD} considers VPD effects on maximum gross photosynthesis,

$$f_{VPD} \;=\; 1 - \alpha_{VPD} * VPD^{\beta_{VPD}}, \qquad \textbf{(7)}$$

where VPD (kPa) is the vapour pressure deficit derived from temperature as in Aber et al. (1996), while α_{VPD} and β_{VPD} are empirical parameters.
We use maximum assimilation from equation (1) to calculate potential photosynthesis considering the light effect (LE_i) and leaf biomass using a 50-layer stratification for the canopy. The variable LAI_i (m^2_{leaf} m^{-2}_{soil}) represents the cumulative leaf area

index at layer i and it is calculated from leaf carbon content. The maximum specific leaf weight ($SLWmax$) and the change in specific leaf weight with canopy mass ($SLWdel$). $SLWmax$ (g$_{\mathrm{DW}}$ m-2$_{\mathrm{leaf}}$) and $SLWdel$ (g$_{\mathrm{DW}}$ m$^{-2}_{\mathrm{leaf}}$ g$^{-1}_{\mathrm{DW}}$) are parameters specific to the plant species,

$$LAI_i = \frac{\frac{C_{TF}}{C_P:DW_P}*0.02}{SLWmax - SLWdel*\, layer_i*\frac{C_{TF}}{C_P:DW_P}*0.02}. \tag{8}$$

The light effect on photosynthesis depends on the light intensity experienced by the foliage layer i (LI_i), which is calculated as a function of photosynthetically active radiation (PAR) and LAI_i,

$$LI_i = PAR *\ e^{K_L * LAI_i}, \tag{9}$$

where PAR (µmol$_{\mathrm{photons}}$·m^{-2} $_{\mathrm{soil}}$ s^{-1}) is scaled with K_L (m$^{2}_{\mathrm{soil}}$ m$^{-2}_{\mathrm{leaf}}$), which is the light attenuation constant that depends on the specific species. Using LI_i, the light effect for each layer is estimated as follows.

$$LE_i = 1 -\ e^{-LI_i * \frac{\ln(2)}{HS}}. \tag{10}$$

The light effect is a value between 0 and 1 (dimensionless) and considers the light half-saturation point expressed as HS (µmol$_{\mathrm{photons}}$·m^{-2} $_{\mathrm{soil}}$ s^{-1}). Based on the previous derivations, potential photosynthesis (PP) (g$_{\mathrm{C}}$ m^{-2} $_{\mathrm{soil}}$ d^{-1}) is calculated by adding each layer contribution.

$$PP = \sum_{i=1}^{50} Amax * LE_i * \frac{C_{TF}}{C_P:DW_P} * 0.02. \tag{11}$$

Potential evapotranspiration (PET) is calculated using PP and considering the water use efficiency (WUE) of the leaf gas exchange process,

$$\mathrm{PET} = PP * \frac{1}{\mathrm{WUE}} * 10^{-6}\ . \tag{12}$$

In equation 12, 10^{-6} is the conversion factor between grams of water and cubic meters of water. Atmospheric CO$_2$ concentration and VPD influences WUE (g$_{\mathrm{C}}$ g^{-1} $_{\mathrm{water}}$) by its effect on conductance,

$$\mathrm{WUE} = \frac{\alpha_{WUE}}{VPD*1000} * 3.67 + \left(1 - f_{CO_2} * \frac{350 * (1 - CL:CA)}{[CO_2]_{atm} * (1 - CL:CA)}\right), \tag{13}$$

Where α_{WUE} (Pa) is a species-specific empirical parameter. Actual evapotranspiration (AET) is the minimum between PET (m$^{3}_{\mathrm{water}}$ m^{-2} $_{\mathrm{soil}}$ d^{-1}) and water available in the soil for tree uptake and is calculated as in Zanchi et al. (2016). Gross primary productivity (GPP) is estimated by scaling PP to AET,

$$GPP = PP * \frac{AET}{\mathrm{PET}}. \tag{14}$$

Carbon synthesized through photosynthesis (i.e., gross primary productivity, GPP) fills a central compartment of labile carbon (C_{LC}), from which it is allocated to four plant labile carbon compartments. Subsequently, carbon from these compartments is transferred to four plant tissue carbon compartments during the growing season. Similarly, other plant nutrients such as nitrogen (N), calcium (Ca), magnesium (Mg), and potassium (K) undergo the same compartmentalization. However, the central labile compartment for these nutrients is replenished through uptake from the soil and is constrained by the maximum storage capacity for each nutrient (Wallman et al., 2005). Carbon allocation may thus be constrained if there is insufficient nutrient availability to meet the specified minimum plant tissue carbon to nutrient ratios, which are fixed parameters in the model Allocation to the foliage labile carbon compartment (AC_{LF}) is implemented as an impulse of carbon at the end of the year. We compute the mass of transferred carbon based on maximum foliage growth ($FGmax$), which factors in the previous year's leaf biomass, light conditions within the canopy, and water availability (Aber et al., 1995). This allocation process is adjusted based on the carbon content in C_{LC} ($\mathrm{g_C\ m^{-2}\ _{soil}}$) at that time, accounting for carbon reserves (CR_P) and minimum branch tissue to foliage tissue ratios ($TB{:}TF$). AC_{LF} ($\mathrm{g_C\ m^{-2}\ _{soil}\ d^{-1}}$) depletes the compartment C_{LC} while increasing the foliage labile carbon compartment that is used for growth in the following season (C_{LF}) ($\mathrm{g_C\ m^{-2}\ _{soil}}$),

$$\mathrm{AC_{LF}} = \frac{\min\left(\mathrm{FGmax}, \frac{\mathrm{C_{LC}}*(1-\mathrm{CR}_P)}{1+TB:TF}\right)}{\Delta \mathrm{t}}. \tag{15}$$

Carbon flow to branch labile compartment ($\mathrm{AC}_{\mathrm{L}B}$) follows a minimum tissue ratio with respect to the leaves and occurs at the beginning of the growing season as,

$$\mathrm{AC_{LB}} = \mathrm{AC_{LF}} * \ TB{:}TF. \tag{16}$$

The growing season commences when the degree days (DD) reach or exceed the species-specific requirements ($GDDmin$) and ends at species-specific parameters ($GDDmax$).

Similarly, carbon flow to wood labile compartment ($\mathrm{AC}_{\mathrm{L}W}$) is computed at the onset of the growing season, determined by the maximum between the minimum for the new foliage ($TW{:}TF$) and the remaining carbon in C_{LC} after accounting for reserves and other allocation flows,

$$\mathrm{AC_{LW}} = \max\left(\mathrm{AC_{LF}} * \ TW{:}TF, \frac{(\mathrm{C_{LC}}*(1-\mathrm{CR}_P)-\mathrm{AC}_{LF}-\mathrm{AC}_{LB}}{\Delta \mathrm{t}}\right). \tag{17}$$

For this contribution we changed the description of carbon allocation to roots (equation 18). Unlike the other compartments, additional carbon for roots ($\mathrm{AC_{LR}}$) can be allocated at any time of the year if the carbon contents in root tissue ($\mathrm{C_{TR}}$) and in the root labile compartment ($\mathrm{C_{LR}}$) are not enough to fulfil the prescribed root to foliage ratio ($\mathrm{TR{:}TF}$). Estimation of the ratio considers both foliage tissue compartment ($\mathrm{C_{TF}}$) and foliage labile compartment ($\mathrm{C_{LF}}$). Carbon reserves are thus used for root allocation, maintenance and growth respiration. Root growth, then, is the minimum between the maximum growth rate constant (G_{TR}) and the root deficit with respect to foliage.

$$\mathrm{PC_{TR}} = \min\left(\mathrm{G_{TR}} * \mathrm{C_{TR}},\ \mathrm{C_{TF}} * \ \mathrm{TR{:}TF} - \mathrm{C_{TR}}\right) \quad \textbf{(18)}$$

During the growing season, the labile carbon compartments are depleted by growth. For foliage and wood, growth kinetics are linear functions of carbon contents in the labile compartments, modulated by degree days (TFf_{GDD}, TWf_{GDD}) based on $GDDmin$ and $GDDmax$ as in Aber et al. (1996), while branches follow foliage growth.

$$\frac{\mathrm{dC_{LF}}}{\mathrm{dt}} = \mathrm{AC_{LF}} - TFf_{GDD} * \mathrm{C_{LF}}\ , \quad \textbf{(19)}$$

$$\frac{\mathrm{dC_{LB}}}{\mathrm{dt}} = \mathrm{AC}_{\mathrm{L}B} - TFf_{GDD} * \mathrm{C_{LF}} * TB{:}TF\ , \quad \textbf{(20)}$$

$$\frac{\mathrm{dC_{LW}}}{\mathrm{dt}} = \mathrm{AC}_{\mathrm{L}W} - TWf_{GDD} * \mathrm{C_{LW}}\ , \quad \textbf{(21)}$$

$$\frac{\mathrm{dC_{LR}}}{\mathrm{dt}} = \mathrm{AC_{LR}} - \mathrm{PC_{TR}}\ . \quad \textbf{(22)}$$

In equations 19 to 22, the first terms of the right side of the equations are the allocation fluxes, occurring only once annually for foliage, branches, and wood (with a value of 0 for other time steps). The second term in equations (19) to (21) represents labile carbon sinks to fuel growth in each plant tissue. Equation (20) is constrained to limit maximum growth to carbon contents in the stock ($\mathrm{C_{LR}}$).

For this contribution, we included the specific tissue's growth respiration cost, therefore total growth respiration (TGR) is estimated by multiplying the second terms of the right side of equations 19 to 22, with the specific tissue's growth respiration cost (RG_P) ($\mathrm{g_C\ g^{-1}_C\ d^{-1}}$) and adding the results.

$$TGR = RG_P * \left(TFf_{GDD} * \mathrm{C_{LF}} * (1 + TB{:}TF\ ) + TWf_{GDD} * \mathrm{C_{LW}} + G_{TR} * \mathrm{C_{TR}}\ \right) \quad \textbf{(23)}$$

The change in the carbon compartments representing plant tissues is then determined by the combination of growth and removals resulting from litterfall and management. Management associated removals are modelled by a rate expressing harvest intensity (HI). Litter production from wood and roots is described with tissue turnover rates (K_i), where i represents plant tissues. While the wood turnover rate constant is fixed, root turnover rates are recalculated annually based on the previous year's nitrogen mineralization, following the method described in Aber et al. (1997).

$$\frac{\mathrm{dC_{TW}}}{\mathrm{dt}} = TWf_{GDD} * \mathrm{C_{LW}} - (HI + \mathrm{K_{TW}}) * \mathrm{C_{TW}}\ , \quad \textbf{(24)}$$

$$\frac{\mathrm{dC_{TR}}}{\mathrm{dt}} = \mathrm{PC_{TR}} - (HI + \mathrm{K_{TR}}) * \mathrm{C_{TR}} \ . \quad \textbf{(25)}$$

Foliage litterfall (L_{TF}) occurs when the day of the year reaches the onset of senescence (OS), and is determined as the minimum between the sum of the mass of foliage layers that photosynthesize less carbon than they respire ($\mathrm{C_{TF}}neg$) and a minimum foliage value determined based on foliage retention (RET),

$$L_{TF} = \frac{\min(\mathrm{C_{TF}}neg, \mathrm{C_{TF}} - RET * \mathrm{C_{TF}})}{\Delta t}, \quad \textbf{(26)}$$

RET ($\mathrm{g_C\ g_C^{-1}}$) is calculated based in latitude as in Ågren et al. (2008). Once L_{TF} ($\mathrm{g_C\ m^{-2}{}_{soil}\ d^{-1}}$) is determined, the mass balances for foliage and branches are expressed as,

$$\frac{\mathrm{dC_{TF}}}{\mathrm{dt}} = TFf_{GDD} * \mathrm{C_{LF}} - L_{TF} - HI * \mathrm{C_{TF}}, \quad \textbf{(27)}$$

$$\frac{dC_{TB}}{dt} = (TFf_{GDD} * C_{LF} - L_{TF} - HI * C_{TF}) * TB{:}TF, \quad \textbf{(28)}$$

where branch litterfall mirrors foliage litterfall dynamics, considering the branch to foliage ratio.

The calculation of maintenance respiration was changed for this contribution by decoupling respiration rates from photosynthesis rates. In this version, we estimate total maintenance respiration (TMR) with tissue-specific (i) linear rates scaled by tissue mass and temperature (RM_i). Temperature response is the same for all tissues, following Aber et al. (1997). In the case of wood and branches, maintenance respiration occurs exclusively in the respiring wood fraction (RWF). Carbon for both growth and maintenance respiration is taken directly from the plant's central labile compartment. The mass balance for the plant's central labile carbon compartment reads

$$\frac{\mathrm{dC_{LC}}}{\mathrm{dt}} = GPP - TMR - TGR - \mathrm{AC_{LF}} - \mathrm{AC_{L\mathit{B}}} - \mathrm{AC_{L\mathit{W}}} - \mathrm{AC_{L\mathit{R}}} - HI * \mathrm{C_{LC}}. \quad \textbf{(29)}$$

If there is not enough carbon for respiration, carbon for the tissue labile compartment will return to $\mathrm{C_{LC}}$. If the deficit persists, the plants die.

1.2 Dead wood and harvested carbon dynamics

Outflows from the wood compartment receive a particular treatment within the model. While the carbon associated with the wood turnover rate is directly sent to the soil as litter, the outflow derived from management removals is divided between dead wood and harvested products. Given its slow dynamics, dead wood (C_{TD}) is defined as a separate compartment containing carbon and nutrients, which are slowly made available to decomposition in the soil through a linear mass transfer rate from dead wood to the soil as litter.

$$\frac{dC_{TD}}{dt} = HI * (1 - HR) * C_{TW} - K_{TD} * C_{TD}, \quad \textbf{(30)}$$

where HR is a dimensionless coefficient that accounts for the fraction of the wood that is transformed into harvested wood products, while what is left (i.e., $1 - \mathrm{HR}$) is sent to the dead wood compartment. K_{TD} is also a rate constant controlling the fraction of dead wood available for decomposition in the soil. Harvest is assumed to occur in one day.

Harvested carbon that does not end up as dead wood enters one of the three carbon compartments that account for typical uses of harvested wood (fuel, paper and hardwood products). These compartments are assumed to follow a first-order exponential decay to account for their final (but delayed) fate as CO_2. The methodology follows IPCC (2006) proposal for harvested wood products, and the mass balance equations for the harvested carbon compartments can be written as,

$$\frac{dC_i}{dt} = HI * HR * \gamma_i * C_{TW} - K_i * C_i, \quad \textbf{(31)}$$

where the subscript index i represents one of the three harvested carbon compartments (HF, HI, HW), γ_i is the fraction of the total harvested carbon that goes into compartment i, and K_i represents the decay rate constant specific to the carbon compartment.

1.3 Soil carbon dynamics

In every soil layer, soil organic matter (SOM) is partitioned into five compartments, with four representing solid organic matter and one representing dissolved organic matter in soil solution (DOM). The four solid compartments are easily decomposable compounds (EDC), cellulose, lignin and peat. Compartments differ in their intrinsic characteristics, such as decomposability. Several chemical elements are tracked within these compartments (C, N, Ca, Mg, K). Therefore, organic carbon—our main focus here—is found in four soil organic carbon compartments (SOC) and as dissolved organic carbon (DOC). Additionally, carbon can be found in the soil in the form of CO_2 and CH_4 whose dynamics are explained in the next section. These compounds may exist in the soil solution or as gases within the unsaturated portion of the soil pore space. The DECOMP model is the foundation for representing soil carbon dynamics (Wallman et al., 2005; Walse et al., 1998).

For this contribution, anaerobic decomposition dynamics were included in the model formulation. Therefore, decomposition occurs via both aerobic and anaerobic pathways and follows first-order kinetics. Decomposition rate constants (TK_i) ($g_C\, g^{-1}_C\, d^{-1}$) for each soil carbon compartment (i) is the sum of the aerobic rate constant (Kae_i) and the anaerobic rate constant (Kan_i) both adjusted for soil temperature, soil water content, and soil solution pH.

$$Kae_i = PKae_i * \mathrm{f_T} * \mathrm{f}_{\theta_w \mathrm{ae}} * \mathrm{f}_{\mathrm{pHae}_i}, \quad \textbf{(32)}$$

$$Kan_i = PKan_i * \mathrm{f_T} * \mathrm{f}_{\theta_w \mathrm{an}} * \mathrm{f}_{\mathrm{pHan}}, \quad \textbf{(33)}$$

$$TK_i = Kae_i + Kan_i. \quad \textbf{(34)}$$

The temperature rate modifier follows an exponential function, increasing by $Q10_x$ every 10°C and reaching a value of one at 30°C as shown in equation (35), where ST is the average daily soil temperature.

$$f_T = \min\left(1, \exp\left(\frac{-\ln(Q10_x)*(30-ST)}{10}\right)\right). \quad \textbf{(35)}$$

The rate modifiers for water content differ between aerobic and anaerobic decomposition pathways. The aerobic function is a piecewise function that grows slowly until the optimum level of water content and then decreases quickly until it reaches 0 at saturation. The anaerobic function is also a piecewise function that is 0 when the soil is drier than the optimum level of water content for the aerobic function and then increases exponentially until reaching 1 at saturation.

$$f_{\theta_{wae}} = \begin{cases} \left(\frac{0.1+FC}{0.1+\theta_{water}}\right) * \left(\frac{\theta_{water}}{FC}\right), & \theta_{water} < FC \\ \left(\frac{FS-\theta_{water}}{FS-FC}\right)^{0.75}, & \theta_{water} \geq FC \end{cases} \quad \textbf{(36)}$$

$$f_{\theta_{wan}} = \begin{cases} 0, & \theta_{water} < FC \\ \left(\frac{\theta_{water}-FC}{FS-FC}\right)^2 * 0.368 * e^{\left(\frac{\theta_{water}-FC}{FS-FC}\right)}, & \theta_{water} \geq FC \end{cases} \quad \textbf{(37)}$$

where θ_{water} represents the volumetric soil water content (m^3_{water} m^{-3}_{soil}), FS denotes the field saturation (m^3_{water} m^{-3}_{soil}), and FC indicates the field capacity (m^3_{water} m^{-3}_{soil}). The function $f_{\theta_{wae}}$ is derived from the methodology proposed by Yan et al. (2018). The function $f_{\theta_{wan}}$ is based on the approach outlined by Tian et al. (2010).

The rate modifier for pH is also defined by two different functions for aerobic and anaerobic decomposition,

$$f_{pHae_i} = \frac{1}{1+\alpha_{pHi}+[H^+]^{\beta_{pH}}}, \quad \textbf{(38)}$$

$$f_{pHan} = 10^{-0.2335*\mathrm{pH}^2+2.7727*\mathrm{pH}-8.6}. \quad \textbf{(39)}$$

In the function f_{pHae_i}, α_{pHi} and β_{pH} represent parameters and $[H^+]$ denotes the concentration of hydrogen ions (Walse et al., 1998) The function f_{pHan} is defined following Meng et al. (2012).

Decomposition flux, denoted DEC_i (g_C $m^{-3}_{soil}d^{-1}$), is calculated by multiplying the adjusted decomposition rate constant by the mass of soil carbon compartments, C_i(g_C m^{-3}_{soil}),

$$DEC_i = TK_i * C_i. \quad \textbf{(40)}$$

The production term for soil carbon compartments (PC_i) originates from litterfall and the decomposition flux of other SOC compartments (equation 41). To simplify the decomposition module, in this contribution, the production terms for EDC, cellulose, and lignin are exclusively associated with litterfall and residues from harvesting.

$$PC_i = \sum_{j=1}^{5} L_j + * \gamma_{ji} + \sum_{j=1}^{4} C_j * HI * (1 - HR) * \gamma_{ji}. \quad \textbf{(41)}$$

The first term represents litterfall (L_j) and is derived for every type of plant tissue and deadwood from equations 24, 25, 27, 28 and 30. The second term is associated with harvesting residues; therefore, deadwood is not considered, and j is equal to four. These fluxes are converted to $g_C\ m^{-3}{}_{soil}\ d^{-1}$ considering soil layer depth and multiplied with the coefficient (γ_{ji}) that determines the fraction of litter from compartment j that enters C_i. In this contribution, for the soil carbon compartments of peat and DOC the production term is associated solely to decomposition fluxes as in equation 42,

$$PC_i = \sum_{i=1}^{5} DEC_i * \frac{Kae_i}{Kae_i + Kan_i} * \left(1 - M_{ae-CO_2}\right) * \gamma_{ji} + \sum_{i=1}^{5} DEC_i * \frac{Kan_i}{Kae_i + Kan_i} * \left(1 - M_{an-CO_2} - M_{an-CH_4}\right) * \gamma_{ji}, \quad \textbf{(42)}$$

where the terms M_{ae-CO_2}, M_{an-CO_2} and M_{an-CH_4}represent mineralized fraction of the decomposition flux and coefficients γ_{ij} are the fractions of the flux from the soil compartment i that enters the soil compartment j. With the previously derived inputs and outputs, the mass balance for the solid SOC compartments i in each layer of soil can be written as,

$$\frac{dC_i}{dt} = PC_i - DEC_i. \quad \textbf{(43)}$$

In the case of DOC compartment (C_{SD}), the mass balance accounts for advection via water percolation and for vertical diffusion between the layers. Therefore, it is necessary to track the concentration of DOC in water, which can be derived from

$$[DOC]_w = \frac{C_{SD}}{\theta_{water}}. \quad \textbf{(44)}$$

For this contribution, we included diffusion of DOC. Diffusivity ($m^2{}_{soil}\ d^{-1}$) is affected by the level of moisture as in Šimůnek & Suarez (1993),

$$D_{SD} = PD_{SD} * \frac{\theta_{water}{}^{\frac{7}{3}}}{FS^2}. \quad \textbf{(45)}$$

Therefore, a mass balance for C_{SD} for each soil layer can be written as an advection-diffusion-reaction equation,

$$\frac{\partial C_{SD}}{\partial t} = PC_{SD} + \frac{\partial Qw * SOC_{DOC}}{\partial z} + \frac{\partial}{\partial z}\left(\theta_w * D_{DOC} * \frac{\partial SOC_{DOC}}{\partial z}\right) - DEC_{SD} - \sum_{k}^{3} \frac{\partial MB_k}{\partial t} * C_{MB}{:}WB_{MB} * \theta_{water}. \quad \textbf{(46)}$$

In equation (46), the first term on the right-hand side is the production term, while the second term is the advection term. Advection of DOC is controlled by water movement represented by Qw ($\mathrm{m^3_{water}\ m^{-2}_{soil}\ d^{-1}}$). By construction, the inflow of water to a specific layer is from the layer above $(l-1)$ or rain in the case of the first layer, while the outflow of water can occur both vertically to the layer below $(l+1)$ and laterally out of the system due to drainage. The third term represents diffusion in the water phase, and the last term represents decomposition per unit soil volume per unit time. The fourth term accounts for the change in biomass of the microbial groups included in nitrogen transformations and the carbon to wet biomass ratio $(C_{MB}\!:\!WB_{MB})$. This is further explained in the section 1.5

1.4 Soil gaseous carbon dynamics

We included a new module that tracks soil gaseous carbon dynamics (CO_2 and CH_4) in this contribution. CO_2 is generated through both anaerobic and aerobic decomposition of soil organic carbon, root respiration, and CH_4 oxidation. Production via decomposition is regulated by the parameter M_i, which represents the inverse of carbon use efficiency (fraction of decomposed carbon that transforms into CO_2 or CH_4). This parameter varies between anaerobic and aerobic decomposition pathways. The respiration fluxes associated with these pathways are defined by partitioning the total flux according to the respective decomposition rate constants (Kae_i and Kan_i) times the parameter M_{ae-CO_2} and M_{an-CO_2}. It may increase if the nitrogen content in organic matter post-carbon mineralization fails to meet microbial stoichiometry requirements, as indicated by fixed microbial biomass C:N ratios, and there is insufficient mineral nitrogen available for immobilization (Manzoni et al., 2010, 2012). Belowground respiration considers the growth and maintenance respiration of root and belowground wood. Methane oxidation follows first-order kinetics. The production term for CO_2 is therefore written as below:

$$PC_{SCO_2} = \frac{RG_P}{z} * (PC_{TR} + TWf_{GDD} * \mathrm{C_{LW}} * BGF_{TW}) + \frac{MR_{TW}}{z} * \mathrm{C_{TW}} * BGF_{TW} + \frac{MR_{TR}}{z} * \mathrm{C_{TR}} + Kmox * \theta_{water} * [CH_4]_w * (1 - \mathrm{f}_{\theta_w \mathrm{an}}) * \mathrm{fmox_T} + \sum_{i=1}^{5} DEC_i * \frac{Kae_i}{Kae_i + Kan_i} * M_{ae-CO_2} + \sum_{i=1}^{5} DEC_i * \frac{Kan_i}{Kae_i + Kan_i} * M_{an-CO_2}. \tag{47}$$

In equation (47), the division by layer depth (z) converts plant respiration fluxes to $\mathrm{g_C\ m^{-3}_{soil} d^{-1}}$. Methane oxidation affects only the methane aqueous concentration, denoted as $[CH_4]_w$ ($\mathrm{g_C\ m^{-3}_{water}}$). The rate of methane oxidation, denoted as $Kmox$ ($\mathrm{d^{-1}}$), is adjusted by the inverse of the water content-dependent function in equation (37), while the temperature function, $\mathrm{f_{Tmox}}$, is defined as in Morel et al. (2019). In the current version of the model, there are no processes that directly consume carbon dioxide. However, carbon dioxide may be transported by advection and diffusion through water and air. Diffusivity is then affected by both soil temperature and water content as follows,

$$D_{SCO_2-air} = \left(PD_{SCO_2-air} + 0.0009 * ST\right) * \frac{\theta_{air}^{\frac{7}{3}}}{FS^2} * CF4\ , \tag{48}$$

$$D_{SCO_2-water} = \left(PD_{SCO_2-water} + 0.0267 * ST + 0.0004 * ST^2\right) * \frac{\theta_{water}^{\frac{7}{3}}}{FS^2} * CF9\ . \tag{49}$$

The influence of water on effective diffusivities (D_{SCO_2-air}, $D_{SCO_2-water}$) is derived from the approach outlined in Šimůnek & Suarez (1993), where θ_a is air content ($m^3_{air}\ m^{-3}_{soil}$). The $CF4$ and $CF9$ are conversion factors to transform potential diffusivities from 10^{-4} $m^2\ s^{-1}$ and 10^{-9} $m^2\ s^{-1}$ (as in the original publications) to $m^2\ d^{-1}$. With these terms, the mass balance equation for CO_2 concentration ($g_C\ m^{-3}_{soil}$) in a given soil layer used within the model is expressed as

$$\frac{\partial[CO_2]_{soil}}{\partial t} = PC_{SCO_2} + \frac{\partial Qw[CO_2]_{water}}{\partial z} + \frac{\partial}{\partial z}\left(\theta_{air} * D_{SCO_2-air} * \frac{\partial[CO_2]_{air}}{\partial z}\right) + \frac{\partial}{\partial z}\left(\theta_{water} * D_{SCO_2-water} * \frac{\partial[CO_2]_{water}}{\partial z}\right). \quad \textbf{(50)}$$

The mass balance equation tracks the CO_2 dynamics, assuming an instantaneous balance between aqueous concentration, denoted $[CO_2]_{water}$ ($g_C\ m^{-3}_{water}$), and the gaseous concentration, denoted $[CO_2]_{air}$ ($g_C\ m^{-3}_{air}$) using Henry's solubility constant. This means that at any time, total concentration, denoted as $[CO_2]_{soil}$ ($g_C\ m^{-3}_{soil}$), can be written as a factor of gaseous concentration using equations (51) and (52).

$$[CO_2]_{soil} = \theta_{water} * [CO_2]_{water} + \theta_{air} * [CO_2]_{air}, \quad \textbf{(51)}$$

$$[CO_2]_{water} = [CO_2]_{air} * H^{cc}_{CO_2} * \left(\frac{ST+273.15}{273.15}\right). \quad \textbf{(52)}$$

A similar approach is used to calculate methane concentration, where the production term is only dependent of decomposition flux,

$$PC_{SCH_4} = \sum_{i=1}^{5} DEC_i * \frac{Kan_i}{Kae_i+Kan_i} * M_{an-CH_4}. \quad \textbf{(53)}$$

Methane transport within the soil involves both advection and diffusion. Diffusivities in water and air are calculated as in equations (48) and (49) using the potential diffusivities of methane (PD_{SCH_4-air}, $PD_{SCH_4-water}$). Water influence is the same as in equations (48) and (49), and temperature influence has the same structure but different parameters as in Morel et al. (2019). Furthermore, the model considers ebullition and plant-mediated transport mechanisms for methane within the soil. Ebullition is based on a concentration threshold approach (Morel et al., 2019). Ebullition ($TG_{CH4-EBU}$) occurs only in soil layers fully saturated, where methane concentration is higher than the concentration threshold,

$$CH_4max = \frac{MR*PS*16.04}{R_{gc}*(ST+273.15)} * 0.748, \quad \textbf{(54)}$$

where MR is the mixing ratio, PS is the soil pressure (atmospheric plus hydrostatic), and R_{gc} is the gas constant. Therefore, the ebullition flux is the difference between the methane concentration in water minus the threshold

$$TG_{CH_4-EBU} = \frac{\max\,(0,[CH_4]_{soil} - CH_4max)}{\Delta t}. \qquad \textbf{(55)}$$

If not all layers within the profile are saturated, the ebullition flux is not released directly into the atmosphere but into the bottom air-filled layer. Plant-mediated transport is modelled as (Raivonen et al., 2017),

$$TG_{CH_4-PMT} = \frac{TRd * A_P * Dair_{CH_4}}{TR\tau} * \frac{[CH_4]_{air} - [CH_4]_{atm}}{z}, \qquad \textbf{(56)}$$

Where A_P is a parameter that can be 0 or 1 and accounts for the presence of aerenchyma in the root system of a given plant species, $TR\tau$ is the root tortuosity, and TRd ($\mathrm{m^2_{root}\ m^{-3}_{soil}}$) is the density of cross-sectional area of root endings at particular soil layer. TRd is calculated in equation (57) with the parameter RCS ($\mathrm{m^2_{root}\ g^{-1}_{DW}}$), which represents the cross-sectional area of root endings per biomass unit, scaled by total root mass as follows,

$$TRd = RCS * \frac{C_{TR}}{C_P{:}DW_P}. \qquad \textbf{(57)}$$

With the previously derived transport, source, and sink terms, a mass balance for methane concentration ($\mathrm{g_C\ m^{-3}_{soil}}$) for any layer in the model can be written as in equation (58),

$$\frac{\partial [CH_4]_{soil}}{\partial t} = PC_{SCH_4} + \frac{\partial Qw[CH_4]_{water}}{\partial z} + \frac{\partial}{\partial z}\left(\theta_{air} * D_{SCH_4-air} * \frac{\partial [CH_4]_{air}}{\partial z}\right) + \frac{\partial}{\partial z}\left(\theta_{water} * D_{SCH_4-water} * \frac{\partial [CH_4]_{water}}{\partial z}\right) - Kmox * \theta_{water} * [CH_4]_w * (1 - \mathrm{f}_{\theta_w \mathrm{an}}) * \mathrm{f_{Tmox}} - TG_{CH_4-EBU} - TG_{CH_4-PMT}\,. \qquad \textbf{(58)}$$

As with CO_2, instant equilibrium between the liquid and gas phases of CH_4 is assumed. Therefore, we apply equations (51) and (52) considering methane's solubility constant ($H^{cc}_{CH_4}$).

1.5 Soil nutrient dynamics

Several other elements besides carbon are simulated through the ecosystem. Nitrogen compounds, magnesium (Mg^+), calcium (Ca^+) and potassium (K^+) are also part of plant compartments and solid organic matter compartments. In soil solution, nitrogen is in the form of ammonium (NH_4^+) and nitrate (NO_3^-), while magnesium, calcium and potassium represent base cations (Bc^+). The model also tracks the concentration of chloride (Cl^-), sodium (Na^+), aluminium (Al^+), and sulphate (SO_4^{-2}). The model estimates pH based on the concentration of these compounds, establishing a relation between hydrogen ions content and the acid neutralizing capacity (ANC) of the soil solution, which is sensitive to CO_2 partial pressure and DOC concentrations. Plant nutrient uptake is based on a maximum plant storage parameter and is limited by root depth and concentration of nutrients. The chemistry module is based on the model SAFE; a detailed model description can be found in Alveteg et al., (1995, 1998), Sverdrup & Warfvinge (1993) and Warfvinge et al. (1993).

For this contribution, nitrogen dynamics have been modified. We adjusted nitrogen mineralization and immobilization according to microbial biomass C:N ratio, organic substrate C:N ratio, and mineral nitrogen availability. Additionally, we have incorporated a representation of nitrification and denitrification processes that explicitly considers microbial biomass and concentration of intermediate nitrogen compounds (NO_2^-, NO, N_2O, N_2).

Nitrogen mineralization (denoted by NM) from soil organic matter decomposition produces ammonium and is associated to the C:N ratio of the decomposition flux and the microbial biomass C:N ratio (Manzoni & Porporato, 2009). We have adapted the previously mentioned principle to both aerobic and anaerobic decomposition flux to calculate net nitrogen mineralization with the following equation:

$$NM_i = \frac{Kae_i}{Kae_i+Kan_i}\left(DEN_i - DEC_i\frac{1-M_{ae-CO_2}}{MCN_{ae}}\right) + \frac{Kan_i}{Kae_i+Kan_i}\left(DEN_i - DEC_i\frac{1-M_{an-CO_2}-M_{an-CH_4}}{MCN_{an}}\right), \qquad \mathbf{(59)}$$

where NM_i (g_N $m^{-3}{}_{soil}d^{-1}$) from compartment i only takes place when the ratio between the carbon decomposition flux (DEC_i) after considering the carbon mineralized fraction and the nitrogen decomposition flux (DEN_i) is more than the C:N ratio of the microbial biomass. When this condition is not met, net nitrogen immobilization of mineral forms of nitrogen (NH_4^+, NO_3^-) is allowed to compensate for the stoichiometric imbalance. If there is not enough mineral nitrogen, an overflow of carbon is simulated by increasing M_{ae-CO_2}, M_{an-CO_2} and M_{an-CH_4} (Schimel and Weintraub, 2003). The C:N ratio of aerobic decomposers (MCN_{an}) is different from that of anaerobic decomposers (MCN_{ae}), therefore, total decomposition flux needs to be scaled to the fraction of aerobic and anaerobic flux.

Mineral nitrogen is also oxidized through nitrification (NH_4^+ to NO_3^-) and reduced by denitrification (NO_3^- to N_2). To model these nitrogen fluxes, we consider ammonium oxidizers, nitrite oxidizers and denitrifiers as in Maggi et al. (2008). Nitrogen transformations follow Monod kinetics; therefore transformation (consumption or production) of a specific nitrogen compound can be written as:

$$NT_i = G_j * \frac{NC_i}{NC_i+M_j} * \frac{MB_k}{Y_j} * \mathrm{f_T} * \mathrm{f}_{\theta_{\mathrm{w}}\mathrm{i}} * \mathrm{f}_{\mathrm{pH}i}, \qquad \mathbf{(60)}$$

In equation (60), the subscript i indicates any of the 5 nitrogen compounds that undergo transformations, the subscript j indicates any of the 6 reactions considered, and the subscript k indicates any of the 3 microbial groups considered. Therefore NT_i (g_N $m^{-3}{}_{water}$ d^{-1}) can be a production or a consumption term in the mass balance of the nitrogen compounds. NC_i is the aqueous concentration of the specific nitrogen compound (g_N $m^{-3}{}_{water}$), G_j is the maximum consumption (d^{-1}) associated to reaction j, M_j is the half saturation constant of the Monod equation (g_N $m^{-3}{}_{water}$), MB_k is the microbial biomass (g_{WB} $m^{-3}{}_{water}$) and MBY_k is a factor converting wet microbial biomass into microbial nitrogen (g_{WB} $g^{-1}{}_N$). Reactions are modified by temperature, water and pH through the rate modifiers $\mathrm{f_T}$, $\mathrm{f}_{\theta_{\mathrm{w}}\mathrm{i}}$, and $\mathrm{f}_{\mathrm{pH}i}$. The temperature rate modifier is the same one used by Li et al. (2000). For denitrification reactions, we use fθan as the rate modifier for water content, while for aerobic processes we use 1-$f_{\theta_w an}$, based on equation (37). The pH rate modifiers are defined as in Bell et al. (2012).

The microbial biomass balance (MB_k) is assumed to satisfy the Monod equation and is written after Tang et al. (2019) as

$$\frac{\partial MB_k}{\partial t} = -K_{MB_k} * MB_k + MBY_k * \sum_{j=1}^{n} NT_i. \tag*{61)}$$

In equation (61), K_{MB_k} is the death rate constant for each microbial group k and n indicates the reactions in which MB_k participates. To account for carbon associated to microbial biomass, we use a simple approach of transforming wet biomass into carbon and including the change of microbial biomass over time within the carbon balance associated to DOC in equation (46). This approach implies that microbial necromass is recycled in the DOC compartment.

1.6 Soil volume dynamics

For the present contribution, we added a dynamic volume approach to the soil profile. The model allows soil layers to expand or shrink according to soil mass changes. It calculates the volume of the solid fraction by relating particle density values with the mass of soil solids. Estimating total soil volume involves relating the volume of solids to a pore to solid ratio. We assume that mineral mass remains stable while adjustments in organic matter mass are made based on decomposition and inputs. The soil volume V_{soil} ($m^3_{soil}\ m^{-2}_{soil}$) in each layer is calculated as,

$$V_{soil} = (1 + P_S : S_S) * \left(\frac{OM_m}{DN_{OM}} + \frac{CY_m}{DN_{CY}} + \frac{SL_m}{DN_{SL}} + \frac{SD_m}{DN_{SD}}\right), \tag*{62)}$$

where CY_m, SL_m, and SD_m are the masses of clay, silt, sand mass ($g_{soil}\ m^{-2}_{soil}$), the porosity is assumed to be fixed via a constant pore to solid ratio $P_S : S_S$ ($m^3_{pores}\ m^{-3}_{solids}$), and also particle density (DN_x) remains constant during the simulation. Therefore, changes in organic matter mass (OM_m) are the only factors causing changes in volume. Soil volume is recalculated at each time step, with adjustments made to concentrations of compounds in soil solution and soil air to account for new distributions of volumetric soil water content and volumetric soil air content. If soil volume expands, we assume that the expansion of pore volume is filled with air. Conversely, if soil volume shrinks and there is sufficient soil air volume, the pore volume loss is assumed to come from soil air volume. Otherwise, water is removed from the system, reducing soil water volume.

1.7 Soil water and soil temperature dynamics

A detailed description of the model representation of soil water dynamics can be found in Wallman et al. (2005) and Zanchi et al. (2016, 2021). In this contribution, we changed infiltration dynamics and we introduced a calculation of groundwater level based on layer saturation above field capacity. Maximum infiltration depth is calculated by integrating the saturated conductivity over the time step $\Delta t K_{sat}$(m_{water}). In the previous version of the model, the parameters field capacity (FC), wilting point (WP) and K_{sat} ($m_{water}\ d^{-1}$) were fixed in time and associated with direct measurements of the parameters themselves or as empirical functions of bulk density. Our dynamic volume approach implies that bulk density changes with time. To make our water dynamics description coherent with volume changes, we use empirical functions derived for drained peatlands to calculate FC, WP and K_{sat} based on values of bulk density (BD). These empirical functions were derived in a metanalysis (Liu et al., 2020, 2022) and are presented in the following equations,

$$WP = 93.55 * (0.20^{BD} * BD^{0.71}) \ , \tag{63}$$

$$FC = 314.86 * (0.12^{BD} * BD^{0.70}) \ , \tag{64}$$

$$K_{sat} = 0.24 * 10^{-2.42 * \log_{10} BD - 2.12} \ . \tag{65}$$

In equations (63), (64) and (65), bulk density is expressed in g cm^{-3}$_{soil}$, FC and WP are expressed in m^{3}$_{water}$ m^{-3}$_{soil}$. The groundwater level (GWL, m$_{water}$) is calculated by adding from the bottom up the thickness of the layers that are fully saturated. Once the iteration finds an unsaturated layer, the depth of water above that layer is calculated as,

$$GWL = \max\left(0, \frac{\theta_w - FC}{FS - FC} * z\right). \tag{66}$$

If the water content θ_w is lower than FC, the water table is as high as the bottom height of the layer; if θ_w is larger than FC, then the depth of water within the layer is proportional to the saturated fraction and the thickness of the layer. The value of GWL of the layer is then added to the thickness of the layers below. If all the layers are saturated, GWL is assumed to be at the surface and have a depth of at least the thickness of the simulated profile. The bottom boundary condition for water transport is imposed by setting the hydraulic conductivity of the bottom layer ($limK_{sat}$).

To simulate temperature in peat soils, we introduced a new module to the model that solves the heat equation assuming conduction dominates heat transfer. We determine the soil layer heat capacity by computing the sum of the product of each constituent's volume fraction (air, water, organic matter and mineral fraction) and its corresponding heat capacity (AHC, WHC, OHC, MHC, respectively) as in Bittelli et al. (2015). The empirical model for peat derived by Zhao et al. (2019) uses three parameters ($\alpha_{HC}, \beta_{HC}, \gamma_{HC}$) and was applied to estimate thermal conductivity. The heat equation is written as,

$$SHC \frac{\partial STK}{\partial t} = \frac{\partial}{\partial z}\left(\lambda \frac{\partial STK}{\partial z}\right). \tag{67}$$

In equation (67), STK is soil temperature in kelvin (K), SHC is the heat capacity (J m^{-3}$_{soil}$ K^{-1}), and λ is the heat conductivity (W m^{-3}$_{soil}$ K^{-1}), which are all dependent of water content. It is worth noticing that we do not include convection terms of heat transfer associated with water movements.

1.8 Numerical implementation

The model comprises several routines solved sequentially with a fixed time step $\Delta t = 1$ day. Firstly, the soil volume is adjusted based on the mass balance from the previous time step. The new volume informs the adjustment of compound concentrations from the preceding time step. Following this, the model estimates potential photosynthesis by considering the climatic conditions of the time step. Once this estimation is complete, the model resolves the water balance, heat dynamics, and gas transport. The water routine constrains actual photosynthesis. Subsequently, the model initiates the plant allocation routine, utilising the determined photosynthesis as its foundation. This routine generates litter, which in turn serves as input for the subsequent decomposition routine. After decomposition, the model solves soil chemistry within the soil solution.

The model generally uses an implicit backwards in time and centred in space discretization scheme. For equations (50), (58) and (67), all soil layers are solved simultaneously by casting the discretised equation into a diagonal matrix and solving it through a gaussian elimination algorithm. For equations (50) and (58), the top boundary condition is given by the atmospheric concentration of the compounds and the bottom boundary condition is given by a zero-flux condition. In equation (55), the terms coming from ebullition are calculated in the previous time step. In equation (67), the top boundary condition is the air temperature affected by snow insulation if present, while the year's average temperature gives the bottom boundary condition. In these three equations, conductivity between layers is a weighted average.

2. Detailed scenario parametrisation.

We tried to avoid extensive calibration and use established parameters as much as possible. Our objective was to use an established plant dynamics (PnET) model coupled with a standard carbon dynamics model in peat soils. Therefore, we only calibrated the fraction of wood that respires (RWF) and the modifier of the bottom layer hydraulic conductivity that controls percolation ($limK_{sat}$) against tree ring data for the period 2007-2009 and GWL data for the period 2008-2013.

2.1 Plant carbon dynamics

Variables used for plant carbon dynamics mentioned in the model description are grouped in Table S1, while parameters and their sources are grouped in Table S2. Most parameters come from articles presenting or applying the PnET model; however, we include new parameters associated with the new developments previously mentioned. Maintenance respiration rate constants (MR_{TF}, MR_{TB}, MR_{TW}, and MR_{TR}) were obtained from Metzler et al. (2024), these parameters are necessary in equation 29. Also, a maximum root growth rate constant is introduced for Equation 18, with a value of 0.05 d-1 derived from the upper range reported for Norway Spruce in a nutrient manipulation study (Sell et al., 2022). As mentioned in section 1.1, the parameter respiring wood fraction (RWF) modulates the maintenance respiration of the woody tissue. The value was obtained by manually calibrating against proxy variables observations related to biomass size (tree ring data from 2007-2009 and GWL data from 2008-2013).

Table S1. Variables for plant carbon dynamics.

Description	**Code**	**Unit**
Maximum Assimilation	Amax	$g_C\ g^{-1}{}_{DW}\ d^{-1}$
Tissue nitrogen foliage compartment	N_{TF}	$g_N\ m^{-2}{}_{soil}$
Tissue carbon foliage compartment	C_{TF}	$g_C\ m^{-2}{}_{soil}$
Day Length	DL	$s\ d^{-1}$
Photosynthesis CO_2 modifier function	f_{CO2}	-
CO_2 atmospheric concentration	$[CO_2]_{atm}$	ppm
Ratio leaf CO_2 concentration to atmospheric CO_2 concentration	CF:CA	-
Photosynthesis temperature modifier function	f_{Tair}	-
Mean daily temperature	Tave	ºC
Photosynthesis VPD modifier function	f_{vpd}	-
Vapor Pressure Deficit	VPD	kPa
Leaf area index	LAI	$m^2{}_{leaf}\ m^{-2}{}_{soil}$
Light Intensity	LI	$\mu mol_{photons}\cdot m^{-2}{}_{soil}\ s^{-1}$
Photosynthetically active radiation	PAR	$\mu mol_{photons}\cdot m^{-2}{}_{soil}\ s^{-1}$
Potential photosynthesis	PP	$g_C\ m^{-2}{}_{soil}\ d^{-1}$
Water use efficiency	WUE	$g_C\ g^{-1}{}_{water}$
Potential evapotranspiration	PET	$m^3{}_{water}\ m^{-2}{}_{soil}\ d^{-1}$
Gross primary productivity	GPP	$g_C\ m^{-2}{}_{soil}\ d^{-1}$
Actual evapotranspiration	AET	$m^3{}_{water}\ m^{-2}{}_{soil}\ d^{-1}$
Plant central carbon compartment	C_{LC}	$g_C\ m^{-2}{}_{soil}$
Maximum foliage growth	FGmax	$g_C\ m^{-2}{}_{soil}$
Foliage retention	RET	$g_C\ g^{-1}{}_C$
Allocation to labile carbon foliage compartment	AC_{LF}	$g_C\ m^{-2}{}_{soil}\ d^{-1}$
Allocation to labile carbon branch compartment	AC_{LB}	$g_C\ m^{-2}{}_{soil}\ d^{-1}$
Allocation to labile carbon wood compartment	AC_{LW}	$g_C\ m^{-2}{}_{soil}\ d^{-1}$
Allocation to labile carbon root compartment	AC_{LR}	$g_C\ m^{-2}{}_{soil}\ d^{-1}$
Labile carbon foliage compartment	C_{LF}	$g_C\ m^{-2}{}_{soil}$
Labile carbon branch compartment	C_{LB}	$g_C\ m^{-2}{}_{soil}$

Description	Code	Unit
Labile carbon wood compartment	C_{LW}	$g_C\ m^{-2}{}_{soil}$
Labile carbon root compartment	C_{LR}	$g_C\ m^{-2}{}_{soil}$
Foliage growth rate based on degree days	TFf_{GDD}	$g_C\ g^{-1}{}_C\ d^{-1}$
Wood growth rate based on degree days	TWf_{GDD}	$g_C\ g^{-1}{}_C\ d^{-1}$
Root production term	PC_{TR}	$g_C\ m^{-2}{}_{soil}\ d^{-1}$
Tissue carbon branch compartment	C_{TB}	$g_C\ m^{-2}{}_{soil}$
Tissue carbon wood compartment	C_{TW}	$g_C\ m^{-2}{}_{soil}$
Tissue carbon root compartment	C_{TR}	$g_C\ m^{-2}{}_{soil}$
Total growth respiration	TGR	$g_C\ d^{-1}$
Root turnover rate	K_{TR}	$g_C\ g^{-1}{}_C\ d^{-1}$
Foliage litterfall	L_{TF}	$g_C\ m^{-2}{}_{soil}\ d^{-1}$
Foliage with a negative carbon balance	$C_{TF}neg$	$g_C\ m^{-2}{}_{soil}$

Table S2. Parameters for plant carbon dynamics.

Description	Code	Unit	Value	Source
Intercept of the maximum photosynthesis rate	α_{Amax}	$nmol_{CO2}\ g^{-1}{}_{DW}\ s^{-1}$	5.3	Aber & Federer, 1992; Zanchi et al., 2021
Slope of the maximum photosynthesis rate	β_{Amax}	$nmol_{CO2}\ g_N\ s^{-1}$	21.5	Aber & Federer, 1992; Zanchi et al., 2021
Daily assimilation as fraction of early morning rate	MR	-	0.76	Aber et al., 1996
Maximum temperature for photosynthesis	PT_{max}	^oC	20	Aber et al., 1996
Minimum temperature for photosynthesis	PT_{min}	^oC	0	Aber et al., 1996
Empirical parameter for VPD effect	α_{VPD}	kPa^{-1}	0.05	Aber et al., 1996
Empirical parameter for VPD effect	β_{VPD}	-	2	Aber et al., 1996
Carbon content in dry weight in plants	$C_P:DW_P$	$g_C\ g^{-1}{}_{DW}$	0.45	Aber et al., 1996
Specific leaf weight	SLWmax	$g_{DW}\ m^{-2}{}_{soil}$	170	Aber et al., 1995
Change of SLW with canopy mass	SLWdel	$g_{DW}\ m^{-2}\ g^{-1}{}_{DW}$	0	Aber et al., 1995
Half saturation point	HS	$\mu mol_{photons}\cdot m^{-2}{}_{soil}\ s^{-1}$	200	Aber et al., 1995
Light attenuation constant	K_L	$m^2{}_{soil}\ m^{-2}{}_{leaf}$	0.4	Dewar et al., 2012
Water use efficiency parameter	α_{WUE}	Pa	10.9	Aber & Federer, 1992; Zanchi et al., 2021

Description	Code	Unit	Value	Source
Plant carbon reserves	CR_P	$g_C\ m^{-2}{}_{soil}$	0.76	Aber & Federer, 1992; Zanchi et al., 2021
Branch to Foliage ratio	TB:TF	$g_C\ g^{-1}{}_C$	0.45	Grote, 2002
Wood to Foliage ratio	TW:TF	$g_C\ g^{-1}{}_C$	0.8	Aber & Federer, 1992; Zanchi et al., 2021
Root to Foliage ratio	TR:TF	$g_C\ g^{-1}{}_C$	0.31	Helmisaari et al., 2007
Growing degrees day at which foliage growth starts	GDDmin	ºC d	300	Aber & Federer, 1992; Zanchi et al., 2021
Growing degrees day at which foliage growth starts	GDDmax	ºC d	1400	Aber & Federer, 1992; Zanchi et al., 2021
Root growth rate	G_{TR}	$g_C\ g^{-1}{}_C\ d^{-1}$	0.05	Sell et al., 2022
Plant growth respiration	RG_P	$g_C\ g^{-1}{}_C\ d^{-1}$	0.25	Aber et al., 1995
Wood turnover rate	K_{TW}	$g_C\ g^{-1}{}_C\ d^{-1}$	6.8E-05	Aber et al., 1997
Onset of senescence	OS	d	270	Zanchi et al., 2016
Foliage maintenance respiration	MR_{TF}	$g_C\ g^{-1}{}_C\ d^{-1}$	0.00173	Metzler et al., 2024
Branch maintenance respiration	MR_{TB}	$g_C\ g^{-1}{}_C\ d^{-1}$	0.00015	Metzler et al., 2024
Wood maintenance respiration	MR_{TW}	$g_C\ g^{-1}{}_C\ d^{-1}$	0.00015	Metzler et al., 2024
Root maintenance respiration	MR_{TR}	$g_C\ g^{-1}{}_C\ d^{-1}$	0.00144	Metzler et al., 2024
Respiring wood fraction	RWF	$g_C\ g^{-1}{}_C$	0.15	Calibrated

2.2 Deadwood and harvested carbon dynamics

Variables used for dead wood and harvested carbon dynamics are grouped in Table S3, while parameters and their sources are grouped in

Table S4. Historical management parameters have already been published (He et al., 2016). The harvest intensity parameter (HI) specifies the proportion of the forest stand that is cut during harvesting, whereas the harvest removal parameter (HR) defines the fraction of the harvested material that is removed from the site. Removals in the future scenario (HI_{2048}, HI_{2079}, HI_{2088}) are assuming the same management pattern as the historical management. The model assumes belowground wood represents 0.2 of the total wood compartment (C_{TW}); therefore, setting the harvest removal parameter (HR) to 0.80 represents the total removal of all aboveground wood during tree harvest. This value represents highly efficient conventional management practice.

Table S3. Variables for dead wood and harvested carbon dynamics.

Description	Code	Unit
Deadwood carbon compartment	C_{TD}	$g_C\ m^{-2}{}_{soil}$
Fuel carbon compartment from harvest	C_{HF}	$g_C\ m^{-2}{}_{soil}$
Paper carbon compartment from harvest	C_{HP}	$g_C\ m^{-2}{}_{soil}$
Hardwood products carbon compartment from harvest	C_{HW}	$g_C\ m^{-2}{}_{soil}$

Table S4. Parameters for dead wood and harvested carbon dynamics.

Description	Code	Unit	Value	Source
Litter transfer rate from deadwood	K_{TD}	$g_C\ g^{-1}{}_C\ d^{-1}$	0.00002	Yu et al., 2018
Harvest intensity in 1979	HI_{1979}	$g_C\ g^{-1}{}_C\ d^{-1}$	0.72	He et al., 2016
Harvest intensity in 2010	HI_{2010}	$g_C\ g^{-1}{}_C\ d^{-1}$	0.10	He et al., 2016
Harvest intensity in 2019	HI_{2019}	$g_C\ g^{-1}{}_C\ d^{-1}$	0.96	Zanchi et al., 2021
Harvest intensity in 2048	HI_{2048}	$g_C\ g^{-1}{}_C\ d^{-1}$	0.72	Assumed
Harvest intensity in 2079	HI_{2079}	$g_C\ g^{-1}{}_C\ d^{-1}$	0.10	Assumed
Harvest intensity in 2088	HI_{2088}	$g_C\ g^{-1}{}_C\ d^{-1}$	0.96	Assumed
Harvest removals	HR	$g_C\ g^{-1}{}_C$	0.80	Assumed
Fraction to fuel	γ_{HF}	$g_C\ g^{-1}{}_C$	0.05	Kasimir et al., 2018
Fraction to paper	γ_{HP}	$g_C\ g^{-1}{}_C$	0.30	Kasimir et al., 2018
Fraction to hardwood products	γ_{HW}	$g_C\ g^{-1}{}_C$	0.65	Kasimir et al., 2018
Decay rate wood for fuel compartment	K_{HF}	$g_C\ g^{-1}{}_C\ d^{-1}$	1	Kasimir et al., 2018
Decay rate wood for paper compartment	K_{HP}	$g_C\ g^{-1}{}_C\ d^{-1}$	0.0010	IPCC, 2006
Decay rate wood for hardwood product compartment	K_{HW}	$g_C\ g^{-1}{}_C\ d^{-1}$	9.0E-05	IPCC, 2006

2.3 Soil carbon dynamics

Variables used for soil carbon dynamics are grouped in Table S5, while parameters and their sources are grouped in Table S6. Most parameters were derived from the original DECOMP model (Wallman et al., 2005; Walse et al., 1998) and recent modifications to ForSAFE (Yu et al., 2018). For this contribution, the previously named recalcitrant SOM compartment was renamed the peat compartment. The aerobic decomposition rate constant was taken from Clymo et al. (1998). This version of the model incorporates anaerobic decomposition based on first-order kinetics, as shown in equation 33. Therefore, we added to anaerobic decomposition rate constants ($PKan_i$) for different soil organic matter compartments. For example, the anaerobic decomposition rate of the EDC compartment ($PKan_{SE}$) has been assumed to be 10% of its aerobic rate, while the anaerobic rate of the cellulose compartment ($PKan_{SC}$) is assumed to be 1%. based on ranges for anaerobic decomposition of polysaccharides in incubation studies (Benner et al., 1984). Limited lignin decomposition is assumed to occur anaerobically; the rate constant ($PKan_{SL}$) is assumed to be 0.01%, informed by Reuter et al. (2024). For peat, the anaerobic decomposition rate constant ($PKan_{SL}$) is derived from catotelm decomposition rate constants (Clymo et al., 1998). Although anaerobic decomposition rate constants are less relevant under drained conditions, they are critical when the model is applied to waterlogged conditions.

The model representation of decomposition does not include an explicit representation of soil microbes in organic matter decomposition. However, microbial contribution to carbon stabilization is implicitly captured via parameters representing the carbon fraction that is not mineralized ($1 - M_{an-CO_2} - M_{an-CH_4}$). The value for the fraction that is not mineralized and goes back into peat from the peat compartment itself ($\gamma_{j\text{-}SP}$) is derived from the value of carbon assimilated into microbial biomass in Yu et al., 2018.

Table S5. Variables for soil carbon dynamics.

Description	**Code**	**Unit**
Total decomposition rate for soil compartment i	TK_i	$g_C\ g^{-1}{}_C\ d^{-1}$
Aerobic decomposition rate for soil compartment i	Kae_i	$g_C\ g^{-1}{}_C\ d^{-1}$
Anaerobic decomposition rate for soil compartment i	Kae_i	$g_C\ g^{-1}{}_C\ d^{-1}$
Decomposition temperature modifier function	f_T	-
Aerobic Decomposition water modifier function	$f_{\theta wae}$	-
Anaerobic Decomposition water modifier function	$f_{\theta wan}$	-
Aerobic Decomposition pH modifier function	f_{pHae}	-
Anaerobic Decomposition pH modifier function	f_{pHan}	-
Soil temperature	ST	^oC
Decomposition carbon flux EDC	DEC_{SE}	$g_C\ m^{-3}{}_{soil}d^{-1}$
Decomposition carbon flux cellulose	DEC_{SC}	$g_C\ m^{-3}{}_{soil}d^{-1}$
Decomposition carbon flux lignin	DEC_{SL}	$g_C\ m^{-3}{}_{soil}d^{-1}$
Decomposition carbon flux peat	DEC_{SP}	$g_C\ m^{-3}{}_{soil}d^{-1}$
Decomposition carbon flux DOM	DEC_{SD}	$g_C\ m^{-3}{}_{soil}d^{-1}$
Soil carbon compartment EDC	C_{SE}	$g_C\ m^{-3}{}_{soil}$
Soil carbon compartment Cellulose	C_{SC}	$g_C\ m^{-3}{}_{soil}$

Description	**Code**	**Unit**
Soil carbon compartment Lignin	C_{SL}	$g_C\ m^{-3}_{soil}$
Soil carbon compartment Peat	C_{SP}	$g_C\ m^{-3}_{soil}$
Soil carbon compartment DOM	C_{SD}	$g_C\ m^{-3}_{soil}$
Litter inflow from branch	L_{TB}	$g_C\ m^{-3}_{soil} d^{-1}$
Litter inflow from wood	L_{TW}	$g_C\ m^{-3}_{soil} d^{-1}$
Litter inflow from root	L_{TR}	$g_C\ m^{-3}_{soil} d^{-1}$
Litter inflow from root	L_{DW}	$g_C\ m^{-3}_{soil} d^{-1}$
Production term associated to EDC	PC_{SE}	$g_C\ m^{-3}_{soil} d^{-1}$
Production term associated to cellulose	PC_{SC}	$g_C\ m^{-3}_{soil} d^{-1}$
Production term associated to lignin	PC_{SL}	$g_C\ m^{-3}_{soil} d^{-1}$
Production term associated to peat	PC_{SP}	$g_C\ m^{-3}_{soil} d^{-1}$
Production term associated to DOM	PC_{SD}	$g_C\ m^{-3}_{soil} d^{-1}$
Diffusivity of DOC	D_{DOC}	$m^2{}_{soil}\ d^{-1}$
Water movement	Q_W	$m^3_{wat}\ m^{-2}{}_{soil}\ d^{-1}$
Concentration of DOC in soil water	$[DOC]_w$	$g_C\ m^{-3}_{water}$

Table S6. Parameters for soil carbon dynamics.

Description	**Code**	**Unit**	**Value**	**Source**
Aerobic Decomposition rate for EDC	$PKae_{SE}$	$g_C\ g^{-1}_C\ d^{-1}$	0.06575	Wallman et al., 2006
Aerobic Decomposition rate for Cellulose	$PKae_{SC}$	$g_C\ g^{-1}_C\ d^{-1}$	0.00301	Wallman et al., 2006
Aerobic Decomposition rate for Lignin	$PKae_{SL}$	$g_C\ g^{-1}_C\ d^{-1}$	0.00046	Wallman et al., 2006
Aerobic Decomposition rate for Peat	$PKae_{SP}$	$g_C\ g^{-1}_C\ d^{-1}$	0.00018	Kleinen et al., 2012
Aerobic Decomposition rate for DOM	$PKae_{SD}$	$g_C\ g^{-1}_C\ d^{-1}$	0.03013	Wallman et al., 2006
Anaerobic Decomposition rate for EDC	$PKan_{SE}$	$g_C\ g^{-1}_C\ d^{-1}$	0.00657	Benner et al., 1984
Anaerobic Decomposition rate for Cellulose	$PKan_{SC}$	$g_C\ g^{-1}_C\ d^{-1}$	0.00003	Benner et al., 1984
Anaerobic Decomposition rate for Lignin	$PKan_{SL}$	$g_C\ g^{-1}_C\ d^{-1}$	4.6E-07	Reuter et al., 2024
Anaerobic Decomposition rate for Peat	$PKan_{SP}$	$g_C\ g^{-1}_C\ d^{-1}$	1.8E-08	Clymo et al., 1998
Anaerobic Decomposition rate for DOM	$PKan_{SD}$	$g_C\ g^{-1}_C\ d^{-1}$	0.00003	Benner et al., 1984

Description	Code	Unit	Value	Source
Aerobic Q10 parameter	$Q10_{ae}$	-	2	Morel et al., 2019
Anaerobic Q10 parameter	$Q10_{an}$	-	4.2	Morel et al., 2019
Parameter for the pH modifier function	β_{pH}	-	1	Walse et al., 1998
Parameter for the pH modifier function	$\alpha_{pH\text{-}SE}$	$kmol_H\ m^{-3}_{water}$	65600	Walse et al., 1998
Parameter for the pH modifier function	$\alpha_{pH\text{-}SC}$	$kmol_H\ m^{-3}_{water}$	20500	Walse et al., 1998
Parameter for the pH modifier function	$\alpha_{pH\text{-}SC}$	$kmol_H\ m^{-3}_{water}$	1050	Walse et al., 1998
Parameter for the pH modifier function	$\alpha_{pH\text{-}SP}$	$kmol_H\ m^{-3}_{water}$	1050	Walse et al., 1998
Parameter for the pH modifier function	$\alpha_{pH\text{-}SD}$	$kmol_H\ m^{-3}_{water}$	20500	Walse et al., 1998
From foliage to soil EDC	$\gamma_{TF\text{-}SE}$	$g_C\ g^{-1}_C$	0.2	Yu et al., 2018
From foliage to soil cellulose	$\gamma_{TF\text{-}SC}$	$g_C\ g^{-1}_C$	0.5	Yu et al., 2018
From foliage to soil lignin	$\gamma_{TF\text{-}SL}$	$g_C\ g^{-1}_C$	0.3	Yu et al., 2018
From branch to soil EDC	$\gamma_{TB\text{-}SE}$	$g_C\ g^{-1}_C$	0.1	Yu et al., 2018
From branch to soil cellulose	$\gamma_{TB\text{-}SC}$	$g_C\ g^{-1}_C$	0.6	Yu et al., 2018
From branch to soil lignin	$\gamma_{TB\text{-}SL}$	$g_C\ g^{-1}_C$	0.3	Yu et al., 2018
From wood to soil EDC	$\gamma_{TW\text{-}SE}$	$g_C\ g^{-1}_C$	0.1	Yu et al., 2018
From wood to soil cellulose	$\gamma_{TW\text{-}SC}$	$g_C\ g^{-1}_C$	0.6	Yu et al., 2018
From wood to soil lignin	$\gamma_{TW\text{-}SL}$	$g_C\ g^{-1}_C$	0.3	Yu et al., 2018
From root to soil EDC	$\gamma_{TR\text{-}SE}$	$g_C\ g^{-1}_C$	0.3	Yu et al., 2018
From root to soil cellulose	$\gamma_{TR\text{-}SC}$	$g_C\ g^{-1}_C$	0.4	Yu et al., 2018
From root to soil lignin	$\gamma_{TR\text{-}SL}$	$g_C\ g^{-1}_C$	0.3	Yu et al., 2018
Partitioning coefficient	$M_{ae\text{-}CO2}$	-	0.6	Manzoni et al., 2018
Partitioning coefficient	$M_{an\text{-}CO2}$	-	0.3	Raivonen et al., 2017
Partitioning coefficient	$M_{an\text{-}CH4}$	-	0.3	Raivonen et al., 2017
From soil compartment j to peat soil compartment	$\gamma_{j\text{-}SP}$	$g_C\ g^{-1}_C$	0.75	Yu et al., 2018
From soil compartment j to DOM compartment	$\gamma_{j\text{-}SD}$	$g_C\ g^{-1}_C$	0.25	Yu et al., 2018
Potential diffusivity of DOC	PD_{SD}	$m^2{}_{soil}\ d^{-1}$	1.1E-05	Camino-Serrano et al., 2018
Carbon to wet biomass for microbes	$C_{MB}:WB_{MB}$	$g_C\ g^{-1}_{WB}$	0.1	Tang et al., 2019

2.4 Soil gaseous carbon dynamics

Variables used for soil gaseous carbon dynamics are grouped in Table S7, while parameters and their sources are grouped in Table S8. Parameters associated with plant-mediated gas transport are not applicable to Norway spruce due to the absence of aerenchyma tissue in its root system. This explains the assigned values for parameters AP, TRτ and RCS in Table S8.

Table S7. Variables for soil carbon dynamics.

Description	**Code**	**Unit**
Temperature function modifier for methane oxidation	$fmox_T$	-
Water diffusivity of CO_2	$D_{SCO2\text{-}air}$	$m^2{}_{soil}\ d^{-1}$
Air diffusivity of CO_2	$D_{SCO2\text{-}water}$	$m^2{}_{soil}\ d^{-1}$
Water diffusivity of CH_4	$D_{SCH4\text{-}air}$	$m^2{}_{soil}\ d^{-1}$
Air diffusivity of CH_4	$D_{SCH4\text{-}water}$	$m^2{}_{soil}\ d^{-1}$
Concentration of compound X in soil	$[X]_{soil}$	$g_C\ m^{-3}{}_{soil}$
Concentration of compound X in soil air	$[X]_{air}$	$g_C\ m^{-3}{}_{air}$
Concentration of compound X in soil water	$[X]_{water}$	$g_C\ m^{-3}{}_{water}$
CO_2 production term	PC_{SCO2}	$g_C\ m^{-3}{}_{soil}d^{-1}$
CH_4 production term	PC_{SCH4}	$g_C\ m^{-3}{}_{soil}d^{-1}$
Threshold for CH_4 ebullition	CH_4max	$g_C\ m^{-3}{}_{soil}$
Pressure at the soil layer	PS	Pa
Ebullition methane flow	$TG_{CH4\text{-}EBU}$	$g_C\ m^{-3}{}_{soil}d^{-1}$
Area of roots	TRd	$m^2{}_{root}\ m^{-3}{}_{soil}$
Plant transport methane flow	$TG_{CH4\text{-}PMT}$	$g_C\ m^{-3}{}_{soil}d^{-1}$

Table S8. Parameters for soil carbon dynamics.

Description	**Code**	**Unit**	**Value**	**Source**
Below ground fraction of wood	BGF_{TW}	-	0.2	Liepiņš et al., 2018
Methane oxidation rate	Kmox	$g_C\ g^{-1}{}_C\ d^{-1}$	0.2	Khvorostyanov et al., 2008
Potential air diffusivity of CO_2	$PD_{SCO2\text{-}air}$	$10^{-4}\ m^2\ s^{-1}$	0.133	Morel et al., 2019
Potential water diffusivity of CO_2	$PD_{SCO2\text{-}water}$	$10^{-9}\ m^2\ s^{-1}$	0.939	Morel et al., 2019
Potential diffusivity of CH_4	$PD_{SCH4\text{-}air}$	$10^{-4}\ m^2\ s^{-1}$	0.188	Morel et al., 2019

Description	Code	Unit	Value	Source
Potential diffusivity of CH_4	$PD_{SCH4\text{-}water}$	$10^{-9}\ m^2\ s^{-1}$	0.980	Morel et al., 2019
HC term for CO_2	H^{CC}_{CO2}	$m^3_{air}\ m^{-3}_{water}$	0.749	Morel et al., 2019
HC term for CH_4	H^{CC}_{CH4}	$m^3_{air}\ m^{-3}_{water}$	0.032	Morel et al., 2019
Mixing ratio	MR	-	0.15	Raivonen et al., 2017
Capacity of the plant to transport gas through roots	A_P	-	0	Estimated
Root tortuosity	$TR\tau$	-	NA	Estimated
Cross-sectional area of root endings per biomass unit	RCS	$m^2_{root}\ g^{-1}_{DW}$	NA	Estimated

2.5 Soil nutrient dynamics

Variables used for soil nutrient dynamics are grouped in Table S9, while parameters and their sources are grouped in Table S10.

Table S9. Variables for soil chemistry dynamics.

Description	Code	Unit
Nitrogen mineralization from soil compartment	NM_{SE}	$g_N\ m^{-3}_{soil} d^{-1}$
Nitrogen mineralization from soil compartment	NM_{SC}	$g_N\ m^{-3}_{soil} d^{-1}$
Nitrogen mineralization from soil compartment	NM_{SL}	$g_N\ m^{-3}_{soil} d^{-1}$
Nitrogen mineralization from soil compartment	NM_{SP}	$g_N\ m^{-3}_{soil} d^{-1}$
Nitrogen mineralization from soil compartment	NM_{SD}	$g_N\ m^{-3}_{soil} d^{-1}$
Decomposition nitrogen flux EDC	DEN_{SE}	$g_N\ m^{-3}_{soil} d^{-1}$
Decomposition nitrogen flux cellulose	DEN_{SC}	$g_N\ m^{-3}_{soil} d^{-1}$
Decomposition nitrogen flux lignin	DEN_{SL}	$g_N\ m^{-3}_{soil} d^{-1}$
Decomposition nitrogen flux peat	DEN_{SP}	$g_N\ m^{-3}_{soil} d^{-1}$
Decomposition nitrogen flux DOM	DEN_{SD}	$g_N\ m^{-3}_{soil} d^{-1}$
Aqueous concentration of nitrogen compound	NC_{NH4}	$g_N\ m^{-3}_{soil}$
Aqueous concentration of nitrogen compound	NC_{NO2}	$g_N\ m^{-3}_{soil}$
Aqueous concentration of nitrogen compound	NC_{NO3}	$g_N\ m^{-3}_{soil}$
Aqueous concentration of nitrogen compound	NC_{NO}	$g_N\ m^{-3}_{soil}$
Aqueous concentration of nitrogen compound	NC_{N2O}	$g_N\ m^{-3}_{soil}$

Description	**Code**	**Unit**
Transformation of mineral nitrogen compound	NT_{NH4}	$g_N\ m^{-3}{}_{soil}d^{-1}$
Transformation of mineral nitrogen compound	NT_{NO2}	$g_N\ m^{-3}{}_{soil}d^{-1}$
Transformation of mineral nitrogen compound	NT_{NO3}	$g_N\ m^{-3}{}_{soil}d^{-1}$
Transformation of mineral nitrogen compound	NT_{NO}	$g_N\ m^{-3}{}_{soil}d^{-1}$
Transformation of mineral nitrogen compound	NT_{N2O}	$g_N\ m^{-3}{}_{soil}d^{-1}$
Biomass ammonium oxidizers	MB_{NIT1}	$g_{WB}\ m^{-3}{}_{soil}$
Biomass nitrite oxidizers	MB_{NIT2}	$g_{WB}\ m^{-3}{}_{soil}$
Biomass denitrifiers	MB_{DEN}	$g_{WB}\ m^{-3}{}_{soil}$

Table S10. Parameters for soil chemistry dynamics.

Description	**Code**	**Unit**	**Value**	**Source**
Microbial CN ratio (aerobic)	MCN_{ae}	$g_C\ g^{-1}{}_N$	11	Manzoni et al., 2010
Microbial CN ratio (anaerobic)	MCN_{an}	$g_C\ g^{-1}{}_N$	30	Reddy & DeLaune, 2008
Maximum growth	G_{oxNH4}	d^{-1}	0.92448	Tang et al., 2019
Michaelis-Menten constant	M_{oxNH4}	$g_N\ m^{-3}{}_{soil}$	4.256	Tang et al., 2019
Yield	Y_{oxNH4}	$g_N\ g^{-1}{}_{WB}$	0.35714	Tang et al., 2019
Maximum growth	G_{oxNO2}	d^{-1}	3.1104	Tang et al., 2019
Michaelis-Menten constant	M_{oxNO2}	$g_N\ m^{-3}{}_{soil}$	4.172	Tang et al., 2019
Yield	Y_{oxNO2}	$g_N\ g^{-1}{}_{WB}$	0.28571	Tang et al., 2019
Maximum growth	G_{reNO3}	d^{-1}	35.1648	Tang et al., 2019
Michaelis-Menten constant	M_{reNO3}	$g_N\ m^{-3}{}_{soil}$	2.898	Tang et al., 2019
Yield	Y_{reNO3}	$g_N\ g^{-1}{}_{WB}$	0.53571	Tang et al., 2019
Maximum growth	G_{reNO2}	d^{-1}	8.36352	Tang et al., 2019
Michaelis-Menten constant	M_{reNO2}	$g_N\ m^{-3}{}_{soil}$	10.486	Tang et al., 2019
Yield	Y_{reNO2}	$g_N\ g^{-1}{}_{WB}$	0.26785	Tang et al., 2019
Maximum growth	G_{reNO}	d^{-1}	69.2064	Tang et al., 2019
Michaelis-Menten constant	M_{reNO}	$g_N\ m^{-3}{}_{soil}$	2.464	Tang et al., 2019
Yield	Y_{reNO}	$g_N\ g^{-1}{}_{WB}$	0.26785	Tang et al., 2019
Maximum growth	G_{reN2O}	d^{-1}	1.45152	Tang et al., 2019

Description	**Code**	**Unit**	**Value**	**Source**
Michaelis-Menten constant	M_{reN2O}	$g_N\ m^{-3}_{soil}$	0.7238	Tang et al., 2019
Yield	Y_{reN2O}	$g_N\ g^{-1}_{WB}$	0.53571	Tang et al., 2019
Death rate ammonium oxidizers	K_{NIT1}	d^{-1}	0.23	Tang et al., 2019
Death rate nitrite oxidizers	K_{NIT2}	d^{-1}	0.13	Tang et al., 2019
Death rate denitrifiers	K_{DEN}	d^{-1}	0.01	Tang et al., 2019

2.6 Soil water and soil temperature dynamics

Variables used for water and temperature dynamics are grouped in Table S11, while parameters and their sources are grouped in

Table S12. We calibrated the modifier of the bottom layer hydraulic conductivity that controls percolation ($LimK_{sat}$) against observations of GWL for the period 2008-2013. This parameter allows water to percolate through the last layer limiting the chances of concentrations of compounds achieving unrealistic values at the bottom of the layer profile. It also affects GWL, which is one of the main carbon regulators in these systems.

Table S11. Variables for water and temperature dynamics.

Description	**Code**	**Unit**
Water content	θ_w	$m^3_{water}\ m^{-3}_{soil}$
Wilting point	WP	$m^3_{water}\ m^{-3}_{soil}$
Field saturation	FS	$m^3_{water}\ m^{-3}_{soil}$
Field capacity	FC	$m^3_{water}\ m^{-3}_{soil}$
Bulk density	BD	$g_{soil}\ m^{-3}_{soil}$
Ground water level	GWL	m_{water}
Saturated hydraulic conductivity	K_{sat}	$m_{water}\ d^{-1}$
Heat capacity	SHC	$J\ m^{-3}_{soil}\ K^{-1}$
Heat conductivity	λ	$W\ m^{-3}_{soil}\ K^{-1}$
Soil temperature in kelvin	STK	K

Table S12. Parameters water and temperature dynamics.

Description	**Code**	**Unit**	**Value**	**Source**
Fraction of the hydraulic conductivity at the bottom layer	$LimK_{sat}$	-	0.018	Calibrated
Air heat capacity	AHC	$J\ m^{-3}_{soil}\ K^{-1}$	$1.23*10^3$	Bittelli et al., 2015
Water heat capacity	WHC	$J\ m^{-3}_{soil}\ K^{-1}$	$4.18*10^6$	Bittelli et al., 2015
Organic matter heat capacity	OCH	$J\ m^{-3}_{soil}\ K^{-1}$	$2.62*10^6$	Bittelli et al., 2015
Mineral heat capacity	MHC	$J\ m^{-3}_{soil}\ K^{-1}$	$2.31*10^6$	Bittelli et al., 2015
Empirical parameter	α_{HC}	-	0.3	Zhao et al., 2019
Empirical parameter	β_{HC}	-	0.87	Zhao et al., 2019
Empirical parameter	γ_{HC}	-	0.6	Zhao et al., 2019

2.5 Soil volume dynamics

Variables used for soil structure dynamics are grouped in Table S13, while parameters and their sources are grouped in Table S14. The pore to solid ratio (inverse of porosity) is derived from on-site observations (Björk et al., 2010), while particle density values are from literature.

Table S13. Variables for soil structure dynamics.

Description	**Code**	**Unit**
Volume of soil layer	V_{soil}	m^3_{soil}
Organic matter mass	OM_m	g_{soil}
Clay mass	CY_m	g_{soil}
Silt mass	SL_m	g_{soil}
Sand mass	SD_m	g_{soil}

Table S14. Parameters for soil structure dynamics.

Description	**Code**	**Unit**	**Value**	**Source**
Particle density organic matter	DN_{OM}	$g_{soil}\ cm^{-3}_{solids}$	1.296	Haan et al., 1994
Particle density clay	DN_{CY}	$g_{soil}\ cm^{-3}_{solids}$	2.657	Haan et al., 1994
Particle density silt	DN_{SL}	$g_{soil}\ cm^{-3}_{solids}$	2.798	Haan et al., 1994
Particle density sand	DN_{SD}	$g_{soil}\ cm^{-3}_{solids}$	2.837	Haan et al., 1994
Pore to solid ratio	$P_S:S_S$	$m^3_{solids}\ m^{-3}_{poros}$	5.61	Björk et al., 2010

References

Aber, J. D. and Federer, C. A.: A generalized, lumped-parameter model of photosynthesis, evapotranspiration and net primary production in temperate and boreal forest ecosystems, Oecologia, 92, 463–474, https://doi.org/10.1007/BF00317837, 1992.

Aber, J. D., Ollinger, S. V., Federer, C. A., Reich, P. B., Goulden, M. L., Kicklighter, D. W., Melillo, J. M., and Lathrop, R. G.: Predicting the effects of climate change on water yield and forest production in the northeastern United States, Climate Research, 5, 207–222, https://doi.org/10.3354/cr005207, 1995.

Aber, J. D., Reich, P. B., and Goulden, M. L.: Extrapolating leaf CO2 exchange to the canopy: a generalized model of forest photosynthesis compared with measurements by eddy correlation, Oecologia, 106, 257–265, https://doi.org/10.1007/BF00328606, 1996.

Aber, J. D., Ollinger, S. V., and Driscoll, C. T.: Modeling nitrogen saturation in forest ecosystems in response to land use and atmospheric deposition, Ecological Modelling, 101, 61–78, https://doi.org/10.1016/S0304-3800(97)01953-4, 1997.

Ågren, G. I., Hyvönen, R., and Nilsson, T.: Are Swedish Forest Soils Sinks or Sources for Co_2—Model Analyses Based on Forest Inventory Data, Biogeochemistry, 89, 139–149, 2008.

Alveteg, M., Sverdrup, H., and Warfvinge, P.: Developing a kinetic alternative in modeling soil aluminium, Water Air Soil Pollut, 79, 377–389, https://doi.org/10.1007/BF01100448, 1995.

Alveteg, M., Walse, C., and Sverdrup, H.: Evaluating simplifications used in regional applications of the SAFE and MAKEDEP models, Ecological Modelling, 107, 265–277, https://doi.org/10.1016/S0304-3800(98)00003-9, 1998.

Andersson, L.: Hydrological Analysis of Basin Behaviour from Soil Moisture Data, Hydrology Research, 19, 1–18, https://doi.org/10.2166/nh.1988.0001, 1988.

Bell, M. J., Jones, E., Smith, J., Smith, P., Yeluripati, J., Augustin, J., Juszczak, R., Olejnik, J., and Sommer, M.: Simulation of soil nitrogen, nitrous oxide emissions and mitigation scenarios at 3 European cropland sites using the ECOSSE model, Nutr Cycl Agroecosyst, 92, 161–181, https://doi.org/10.1007/s10705-011-9479-4, 2012.

Benner, R., Maccubbin, A. E., and Hodson, R. E.: Anaerobic biodegradation of the lignin and polysaccharide components of lignocellulose and synthetic lignin by sediment microflora, Appl Environ Microbiol, 47, 998–1004, https://doi.org/10.1128/aem.47.5.998-1004.1984, 1984.

Bergström, S.: Principles and Confidence in Hydrological Modelling, Hydrology Research, 22, 123–136, https://doi.org/10.2166/nh.1991.0009, 1991.

Bittelli, M., Campbell, G. S., and Tomei, F.: Soil Temperature and Heat Flow, in: Soil Physics with Python: Transport in the Soil–Plant–Atmosphere System, edited by: Bittelli, M., Campbell, G. S., and Tomei, F., Oxford University Press, 0, https://doi.org/10.1093/acprof:oso/9780199683093.003.0004, 2015.

Björk, R. G., Ernfors, M., Sikström, U., Nilsson, M. B., Andersson, M. X., Rütting, T., and Klemedtsson, L.: Contrasting effects of wood ash application on microbial community structure, biomass and processes in drained forested peatlands, FEMS Microbiology Ecology, 73, 550–562, https://doi.org/10.1111/j.1574-6941.2010.00911.x, 2010.

Camino-Serrano, M., Guenet, B., Luyssaert, S., Ciais, P., Bastrikov, V., De Vos, B., Gielen, B., Gleixner, G., Jornet-Puig, A., Kaiser, K., Kothawala, D., Lauerwald, R., Peñuelas, J., Schrumpf, M., Vicca, S., Vuichard, N., Walmsley, D., and Janssens, I. A.: ORCHIDEE-SOM: modeling soil organic carbon (SOC) and dissolved organic carbon (DOC) dynamics along vertical soil profiles in Europe, Geoscientific Model Development, 11, 937–957, https://doi.org/10.5194/gmd-11-937-2018, 2018.

Clymo, R. S., Turunen, J., and Tolonen, K.: Carbon Accumulation in Peatland, Oikos, 81, 368–388, https://doi.org/10.2307/3547057, 1998.

Dewar, R. C., Tarvainen, L., Parker, K., Wallin, G., and McMurtrie, R. E.: Why does leaf nitrogen decline within tree canopies less rapidly than light? An explanation from optimization subject to a lower bound on leaf mass per area, Tree Physiology, 32, 520–534, https://doi.org/10.1093/treephys/tps044, 2012.

Grote, R.: Foliage and branch biomass estimation of coniferous and deciduous tree species, Silva Fennica, 36, 2002.

Haan, C. T., Barfield, B. J., and Hayes, J. C.: 7 - Sediment Properties and Transport, in: Design Hydrology and Sedimentology for Small Catchments, edited by: Haan, C. T., Barfield, B. J., and Hayes, J. C., Academic Press, San Diego, 204–237, https://doi.org/10.1016/B978-0-08-057164-5.50011-6, 1994.

He, H., Jansson, P.-E., Svensson, M., Björklund, J., Tarvainen, L., Klemedtsson, L., and Kasimir, Å.: Forests on drained agricultural peatland are potentially large sources of greenhouse gases – insights from a full rotation period simulation, Biogeosciences, 13, 2305–2318, https://doi.org/10.5194/bg-13-2305-2016, 2016.

Helmisaari, H.-S., Derome, J., Nöjd, P., and Kukkola, M.: Fine root biomass in relation to site and stand characteristics in Norway spruce and Scots pine stands, Tree Physiol, 27, 1493–1504, https://doi.org/10.1093/treephys/27.10.1493, 2007.

IPCC: IPCC Guidelines for National Greenhouse Gas Inventories, Prepared by the National Greenhouse Gas Inventories Programme, Eggleston H.S., Buendia L., Miwa K., Ngara T. and Tanabe K. (eds)., IGES, Japan, 2006.

Kasimir, Å., He, H., Coria, J., and Nordén, A.: Land use of drained peatlands: Greenhouse gas fluxes, plant production, and economics, Global Change Biology, 24, 3302–3316, https://doi.org/10.1111/gcb.13931, 2018.

Khvorostyanov, D. V., Krinner, G., Ciais, P., Heimann, M., and Zimov, S. A.: Vulnerability of permafrost carbon to global warming. Part I: model description and role of heat generated by organic matter decomposition, Tellus B, 60, 250–264, https://doi.org/10.1111/j.1600-0889.2007.00333.x, 2008.

Li, C., Aber, J., Stange, F., Butterbach-Bahl, K., and Papen, H.: A process-oriented model of N2O and NO emissions from forest soils: 1. Model development, Journal of Geophysical Research: Atmospheres, 105, 4369–4384, https://doi.org/10.1029/1999JD900949, 2000.

Liepiņš, J., Lazdiņš, A., and Liepiņš, K.: Equations for estimating above- and belowground biomass of Norway spruce, Scots pine, birch spp. and European aspen in Latvia, Scandinavian Journal of Forest Research, 33, 58–70, https://doi.org/10.1080/02827581.2017.1337923, 2018.

Liu, H., Price, J., Rezanezhad, F., and Lennartz, B.: Centennial-Scale Shifts in Hydrophysical Properties of Peat Induced by Drainage, Water Resources Research, 56, e2020WR027538, https://doi.org/10.1029/2020WR027538, 2020.

Liu, H., Rezanezhad, F., and Lennartz, B.: Impact of land management on available water capacity and water storage of peatlands, Geoderma, 406, 115521, https://doi.org/10.1016/j.geoderma.2021.115521, 2022.

Maggi, F., Gu, C., Riley, W. J., Hornberger, G. M., Venterea, R. T., Xu, T., Spycher, N., Steefel, C., Miller, N. L., and Oldenburg, C. M.: A mechanistic treatment of the dominant soil nitrogen cycling processes: Model development, testing, and application, Journal of Geophysical Research: Biogeosciences, 113, https://doi.org/10.1029/2007JG000578, 2008.

Manzoni, S. and Porporato, A.: Soil carbon and nitrogen mineralization: Theory and models across scales, Soil Biology and Biochemistry, 41, 1355–1379, https://doi.org/10.1016/j.soilbio.2009.02.031, 2009.

Manzoni, S., Trofymow, J. A., Jackson, R. B., and Porporato, A.: Stoichiometric controls on carbon, nitrogen, and phosphorus dynamics in decomposing litter, Ecol. Monogr., 80, 89–106, https://doi.org/10.1890/09-0179.1, 2010.

Manzoni, S., Taylor, P., Richter, A., Porporato, A., and Ågren, G. I.: Environmental and stoichiometric controls on microbial carbon-use efficiency in soils, New Phytologist, 196, 79–91, https://doi.org/10.1111/j.1469-8137.2012.04225.x, 2012.

Manzoni, S., Čapek, P., Porada, P., Thurner, M., Winterdahl, M., Beer, C., Brüchert, V., Frouz, J., Herrmann, A. M., Lindahl, B. D., Lyon, S. W., Šantrůčková, H., Vico, G., and Way, D.: Reviews and syntheses: Carbon use efficiency from organisms to ecosystems – definitions, theories, and empirical evidence, Biogeosciences, 15, 5929–5949, https://doi.org/10.5194/bg-15-5929-2018, 2018.

Meng, L., Hess, P. G. M., Mahowald, N. M., Yavitt, J. B., Riley, W. J., Subin, Z. M., Lawrence, D. M., Swenson, S. C., Jauhiainen, J., and Fuka, D. R.: Sensitivity of wetland methane emissions to model assumptions: application and model testing against site observations, Biogeosciences, 9, 2793–2819, https://doi.org/10.5194/bg-9-2793-2012, 2012.

Metzler, H., Launiainen, S., and Vico, G.: Amount of carbon fixed, transit time and fate of harvested wood products define the climate change mitigation potential of boreal forest management—A model analysis, Ecological Modelling, 491, 110694, https://doi.org/10.1016/j.ecolmodel.2024.110694, 2024.

Morel, X., Decharme, B., Delire, C., Krinner, G., Lund, M., Hansen, B. U., and Mastepanov, M.: A New Process-Based Soil Methane Scheme: Evaluation Over Arctic Field Sites With the ISBA Land Surface Model, Journal of Advances in Modeling Earth Systems, 11, 293–326, https://doi.org/10.1029/2018MS001329, 2019.

Raivonen, M., Smolander, S., Backman, L., Susiluoto, J., Aalto, T., Markkanen, T., Mäkelä, J., Rinne, J., Peltola, O., Aurela, M., Lohila, A., Tomasic, M., Li, X., Larmola, T., Juutinen, S., Tuittila, E.-S., Heimann, M., Sevanto, S., Kleinen, T., Brovkin, V., and Vesala, T.: HIMMELI v1.0: HelsinkI Model of MEthane buiLd-up and emIssion for peatlands, Geoscientific Model Development, 10, 4665–4691, https://doi.org/10.5194/gmd-10-4665-2017, 2017.

Reddy, K. R. and DeLaune, R. D.: Carbon, in: Biogeochemistry of Wetlands, CRC Press, 2008.

Reuter, J., Reuter, H., and Zak, D.: Decomposition of lignin and carbohydrates in a rewetted peatland: a comparative analysis of surface water and anaerobic soil layers, Biogeochemistry, 167, 545–561, https://doi.org/10.1007/s10533-023-01102-2, 2024.

Schimel, J. P. and Weintraub, M. N.: The implications of exoenzyme activity on microbial carbon and nitrogen limitation in soil: a theoretical model, Soil Biology and Biochemistry, 35, 549–563, https://doi.org/10.1016/S0038-0717(03)00015-4, 2003.

Sell, M., Smith, A. G., Burdun, I., Rohula-Okunev, G., Kupper, P., and Ostonen, I.: Assessing the fine root growth dynamics of Norway spruce manipulated by air humidity and soil nitrogen with deep learning segmentation of smartphone images, Plant Soil, 480, 135–150, https://doi.org/10.1007/s11104-022-05565-4, 2022.

Šimůnek, J. and Suarez, D. L.: Modeling of carbon dioxide transport and production in soil: 1. Model development, Water Resources Research, 29, 487–497, https://doi.org/10.1029/92WR02225, 1993.

Sverdrup, H. and Warfvinge, P.: Calculating field weathering rates using a mechanistic geochemical model PROFILE, Applied Geochemistry, 8, 273–283, https://doi.org/10.1016/0883-2927(93)90042-F, 1993.

Tang, F. H. M., Riley, W. J., and Maggi, F.: Hourly and daily rainfall intensification causes opposing effects on C and N emissions, storage, and leaching in dry and wet grasslands, Biogeochemistry, 144, 197–214, 2019.

Tian, H., Xu, X., Liu, M., Ren, W., Zhang, C., Chen, G., and Lu, C.: Spatial and temporal patterns of CH_4 and N_2O fluxes in terrestrial ecosystems of North America during 1979–2008: application of a global biogeochemistry model, Biogeosciences, 7, 2673–2694, https://doi.org/10.5194/bg-7-2673-2010, 2010.

Wallman, P., Svensson, M. G. E., Sverdrup, H., and Belyazid, S.: ForSAFE—an integrated process-oriented forest model for long-term sustainability assessments, Forest Ecology and Management, 207, 19–36, https://doi.org/10.1016/j.foreco.2004.10.016, 2005.

Wallman, P., Belyazid, S., Svensson, M. G. E., and Sverdrup, H.: DECOMP – a semi-mechanistic model of litter decomposition, Environmental Modelling & Software, 21, 33–44, https://doi.org/10.1016/j.envsoft.2004.09.026, 2006.

Walse, C., Berg, B., and Sverdrup, H.: Review and synthesis of experimental data on organic matter decomposition with respect to the effect of temperature, moisture, and acidity, Environ. Rev., 6, 25–40, https://doi.org/10.1139/a98-001, 1998.

Warfvinge, P., Falkengren-Grerup, U., Sverdrup, H., and Andersen, B.: Modelling long-term cation supply in acidified forest stands, Environmental Pollution, 80, 209–221, https://doi.org/10.1016/0269-7491(93)90041-L, 1993.

Yan, Z., Bond-Lamberty, B., Todd-Brown, K. E., Bailey, V. L., Li, S., Liu, C., and Liu, C.: A moisture function of soil heterotrophic respiration that incorporates microscale processes, Nat Commun, 9, 2562, https://doi.org/10.1038/s41467-018-04971-6, 2018.

Yu, L., Zanchi, G., Akselsson, C., Wallander, H., and Belyazid, S.: Modeling the forest phosphorus nutrition in a southwestern Swedish forest site, Ecological Modelling, 369, 88–100, https://doi.org/10.1016/j.ecolmodel.2017.12.018, 2018.

Zanchi, G., Belyazid, S., Akselsson, C., Yu, L., Bishop, K., Köhler, S. J., and Grip, H.: A Hydrological Concept including Lateral Water Flow Compatible with the Biogeochemical Model ForSAFE, Hydrology, 3, 11, https://doi.org/10.3390/hydrology3010011, 2016.

Zanchi, G., Yu, L., Akselsson, C., Bishop, K., Köhler, S., Olofsson, J., and Belyazid, S.: Simulation of water and chemical transport of chloride from the forest ecosystem to the stream, Environmental Modelling & Software, 138, 104984, https://doi.org/10.1016/j.envsoft.2021.104984, 2021.

Zhao, Y., Si, B., Zhang, Z., Li, M., He, H., and Hill, R. L.: A new thermal conductivity model for sandy and peat soils, Agricultural and Forest Meteorology, 274, 95–105, https://doi.org/10.1016/j.agrformet.2019.04.004, 2019.